

Original paper

# Variscan thermal overprints exemplified by U–Th–Pb monazite and K–Ar muscovite and biotite dating at the eastern margin of the Bohemian Massif (East Sudetes, Czech Republic)

Karel SCHULMANN<sup>1,2\*</sup>, Emilien OLIOT<sup>2</sup>, Monika KOŠULIČOVÁ<sup>1</sup>, Raymond MONTIGNY<sup>2</sup>, Pavla ŠTÍPSKÁ<sup>1,2</sup>

<sup>1</sup> Czech Geological Survey, Klárov 3, 118 21 Prague 1, Czech Republic; [schulmann.karel@gmail.com](mailto:schulmann.karel@gmail.com)

<sup>2</sup> Institut de Physique du Globe de Strasbourg; UMR 7516, University of Strasbourg/EOST, CNRS; 1 rue Blessig, F-67084 Strasbourg Cedex, France

\*Corresponding author



Potassium–argon method on muscovite and biotite and chemical U–Th–Pb method on monazite have been used to date various tectonic and thermal processes affecting the Silesian orogenic wedge at the eastern Variscan front (NE Bohemian Massif). This wedge is composed of three structural units showing an increasing Barrovian metamorphic gradient from the east to the west and LP–HT reworking related to voluminous granite intrusion of the Žulová Pluton in the central part. Three groups of ages are reported: 1) Mississippian (340–320 Ma) K–Ar muscovite ages from the western kyanite zone and easternmost biotite–chlorite zone, ~320 Ma U–Th–Pb ages of monazite inclusions in syn-burial  $S_1$  fabric preserved in garnets of the kyanite zone, 2) Pennsylvanian–Early Permian (~310–290 Ma) K–Ar ages on muscovite and biotite and matrix monazite from the sillimanite and staurolite zones of the central part of the wedge, 3) Early to Mid-Permian K–Ar muscovite and biotite and U–Th–Pb matrix monazite ages (~280–260 Ma) from the southern part of the area, adjacent to the Sudetic fault system. The sequence of obtained ages is interpreted as reflecting the Mississippian formation of the Silesian orogenic wedge that was followed by crustal-scale detachment related to Pennsylvanian–Early Permian intrusion of a voluminous Žulová Pluton accompanied by important fluid flow. Finally, the southern part of the studied domain was probably reworked by Permian fault system associated with renewed fluid activity.

**Keywords:** Monazite dating, K–Ar geochronology, Silesian Domain, thermal overprints, Bohemian Massif

**Received:** 16 March 2014; **accepted:** 3 November 2014; **handling editor:** F. Finger

## 1. Introduction

The cooling histories of metamorphic terrains provide important information about the exhumation processes and their timing. They can be constrained by using various thermochronological techniques and their combinations, for example by the K–Ar or <sup>40</sup>Ar–<sup>39</sup>Ar dating on micas (e.g. McDougall and Harrison 1988) and chemical U–Th–Pb dating on monazite (CHIME; e.g. Montel et al. 1996). While the first method allows determining timing of cooling through closure temperatures of *c.* 300–450 °C, the second one reveals time of monazite (re)crystallization (e.g. Crowley and Ghent 1999; Cherniak et al. 2004; Gardés et al. 2007; Williams et al. 2011; Kelly et al. 2012 and references therein). Therefore, monazites armoured in garnet or other prograde porphyroblasts may provide age constraints on the prograde part of the metamorphic history (Bell and Welch 2002), while grains of the same mineral in the matrix may be a product of decompression reactions (Gibson et al. 2004) or fluid circulation (Seydoux-Guillaume et al. 2002).

Schulmann and Gayer (2000) proposed a model of Early Carboniferous continental underthrusting of the Brunia basement underneath the Orlica–Śnieżnik Dome (OSD). They suggested that the continental underthrusting of the three crustal boudins was responsible for the formation of the Silesian orogenic wedge and Barrovian metamorphic zonation (Košuličová and Štípská 2007) by analogy to similar metamorphic pattern described in southerly Svratka and Thaya tectonic windows (Štípská and Schulmann 1995; Štípská et al. 2000; Ulrich et al. 2002). The time scales of this underthrusting have been estimated using the formation age of the deep Culm foreland basin in the east and the age of burial and Early Carboniferous exhumation/cooling of orogenic lower crust in the adjacent high-grade rocks of the OSD. Here, the prograde metamorphic history of the OSD and the Staré Město Belt may have extended to Late Devonian (Gordon et al. 2005; Bröcker et al. 2009, 2010; Jastrzębski et al. 2013). The timing of exhumation of the OSD has been recently estimated at 342–335 Ma using <sup>40</sup>Ar–<sup>39</sup>Ar method (Schneider et al. 2006; Chopin et al. 2012) and at 340–330 Ma using U–Th–Pb on monazite (Gordon

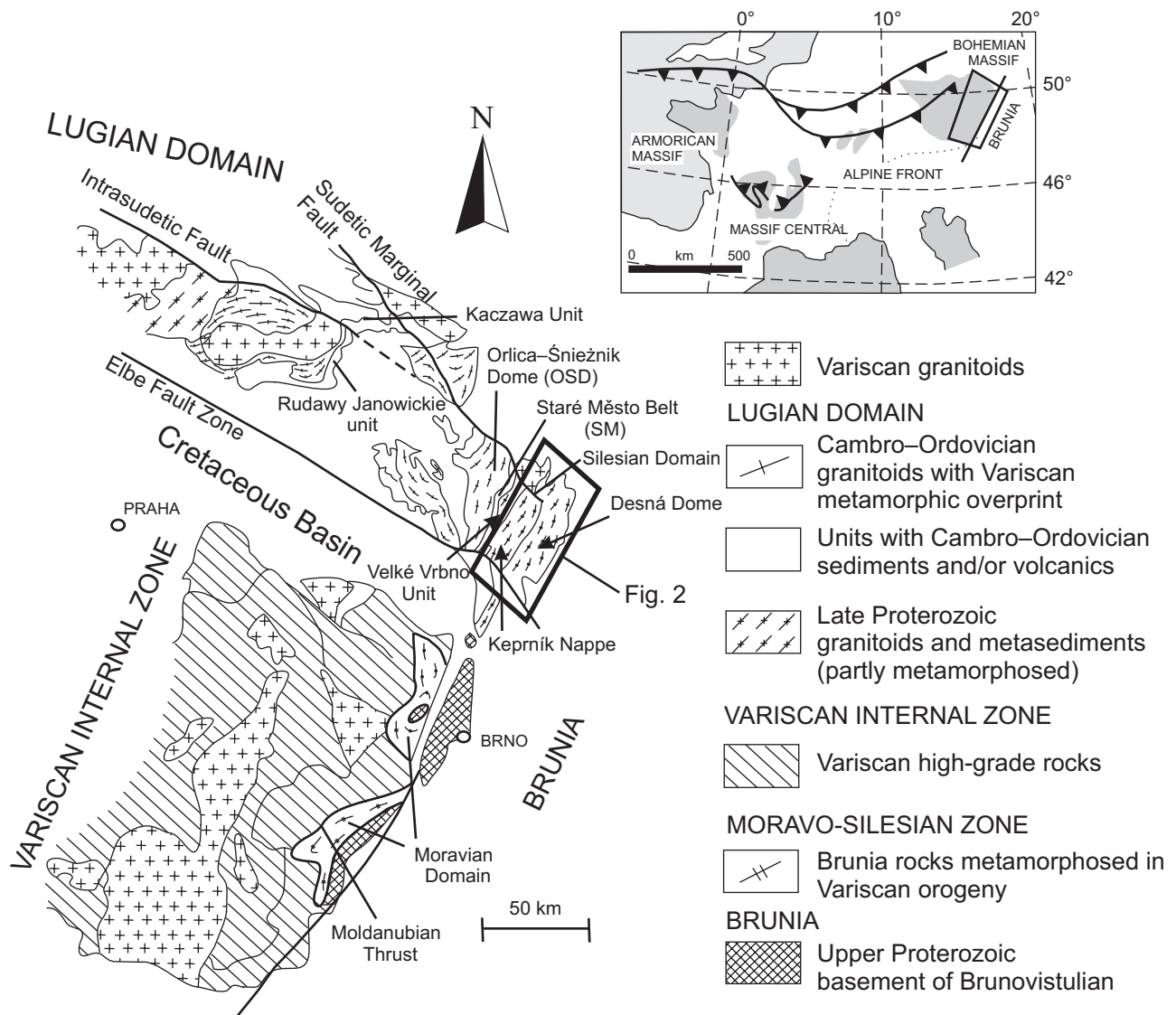


**Fig. 1** Outline geological map of the Bohemian Massif with location of the studied area – Silesian Domain. Top right inset shows position of the Bohemian Massif in the framework of the European Variscides. The black frame indicates the studied area.

et al. 2005; Kusiak et al. 2008), which contrasts with younger 310–300 Ma  $^{40}\text{Ar}$ – $^{39}\text{Ar}$  ages of Maluski et al. (1995) reported from the Silesian Domain. Therefore, the main problem addressed in this work is the significance of highly controversial ages from the Silesian Domain that appear to be younger than those of the adjacent OSD rocks and also of the southerly Svatka and Thaya domes of the Moravian Zone (335–325 Ma, Dallmeyer et al. 1992; Fritz et al. 1996).

In order to fill the gap, U–Th–Pb *in situ* electron-microprobe dating on monazite (Montel et al. 1996) and K–Ar dating on biotite and muscovite (e.g. McDougall and Harrison 1988) were applied to study the timing of metamorphism and cooling of the Silesian orogenic wedge at the eastern margin of the Bohemian Massif. These data are used to discuss the tectonic significance

of the difference in the cooling ages from the Orlica–Šniežnik Dome and the Silesian orogenic wedge.

## 2. Geological setting and previous geochronology

### 2.1. Geology of the eastern margin of the Bohemian Massif

A 300 km long Variscan front (Fig. 1), marked by the boundary between the internal and external orogenic domains, forms the eastern margin of the Bohemian Massif. The internal domain characterized by the presence of high-grade metamorphic rocks is interpreted as an exhumed orogenic root of the Variscan belt, called the

Moldanubian Domain in the south, and the Lugian Domain in the north (Suess 1926). The latter is represented by high-grade rocks of the Orlica–Śnieżnik Dome. To the east occurs the external Brunia microcontinent (Dudek 1980) that was underthrust below the Moldanubian gneisses and migmatites in Carboniferous times (Schulmann et al. 1994, Schulmann et al. 2008). Its western metamorphosed and imbricated part, the Moravo–Silesian Zone, emerges in the form of three tectonic windows, the Thaya and Svatka windows forming the Moravian branch of the zone in the south, and the Silesian Domain in the north (Suess 1912). The major thrust separating the internal and external domains in the south is known as the Moldanubian thrust. The exact position of Brunovistulian boundary in the north is a matter of discussion because of differently interpreted significance of the Silesian Domain boundary (e.g. Jastrzębski 2012). The eastern margin of the OSD is rather well defined, though (e.g. Don et al. 2003).

The southerly Moldanubian Domain and Moravian Zone are separated from the northerly OSD and Silesian Domain by the dextral Elbe Fault Zone (Fig. 1). This lithospheric-scale transcurrent fault zone belongs to dextral fault system dissecting the whole Variscan Europe during the Late Carboniferous and Permian (the Bray, the Pfahl–Danube and the Sudetic fault systems; Edel et al. 2003, 2013). This fault system strongly affected the Silesian Domain and the southern and northern margins of the OSD. The second conjugate fault system reactivated the Moldanubian–Moravian boundary and is represented by N–S trending sinistral faults like the Diendorf Fault Zone in Austria (Hejl et al. 2003). Related was formation of Permian basins such as the Boskovice Furrow in the south or Krkonoše Piedmont Basin in the west (Martínek and Štolfová 2009).

## 2.2. The Silesian Domain

The present geology of the Silesian Domain is interpreted as a result of three major tectonic events. The Devonian rifting was a reason for the formation of three crustal-scale boudins (the Desná Dome, the Keprník Nappe and the Velké Vrbno Unit) that formed on a Neoproterozoic basement, and for the development of sedimentary basins between them (Chlupáč 1989, 1994). Schulmann and Gayer (2000) proposed that an Early Carboniferous oblique compression caused the successive underthrusting of the crustal boudins to the west, resulting in the formation of an orogenic wedge with westward increasing grade of Barrovian-type metamorphism (Souček 1978; Baratoux et al. 2005; Košuličová and Štípská 2007). A Late Carboniferous event was marked by the extrusion and exhumation of the wedge in a transpressional regime (Schulmann and Gayer 2000). Subsequent intrusion of the Žulová Pluton (Fig. 2) was associated with the local

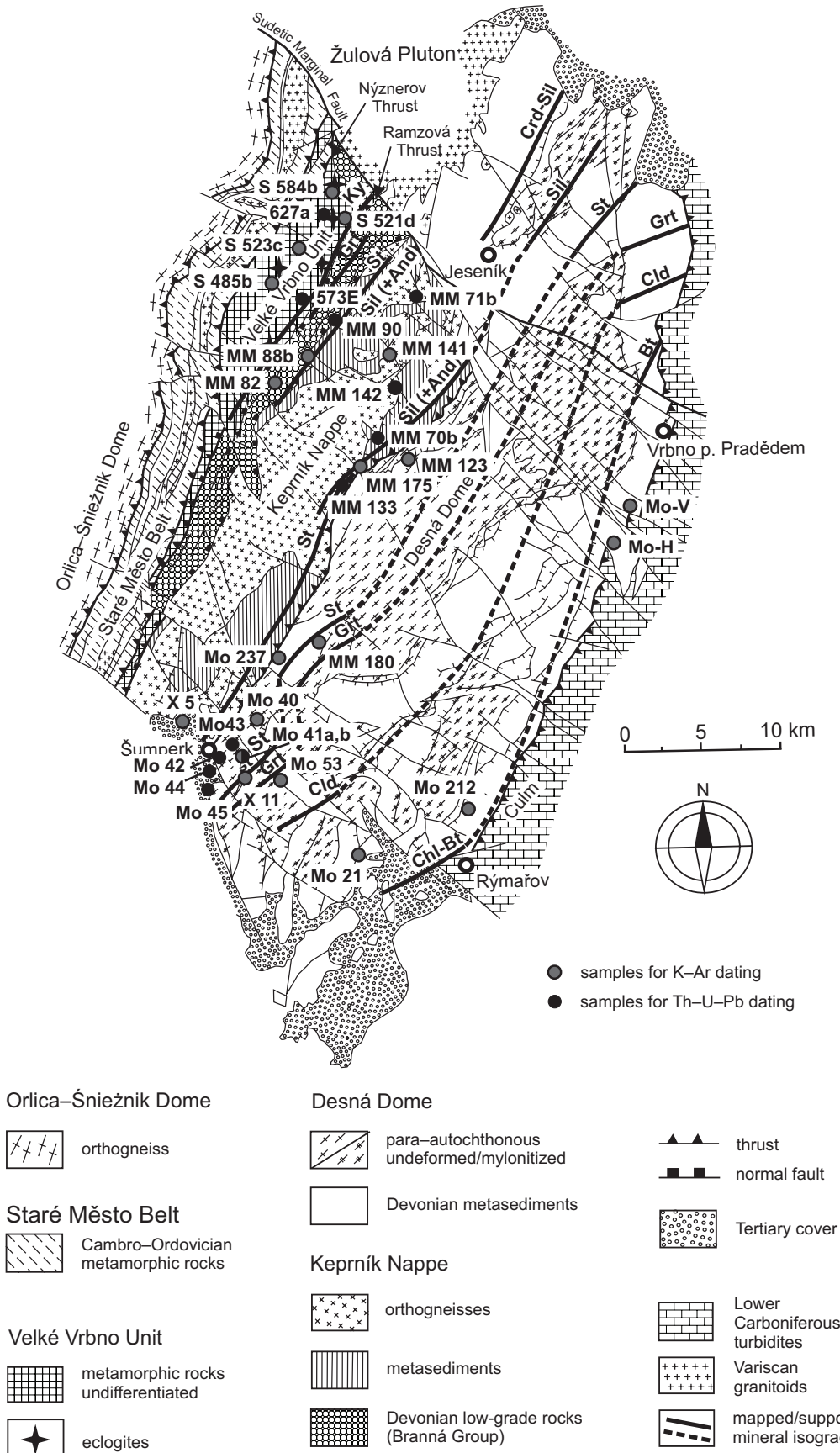
extension and HT–LP metamorphism at the western part of the Silesian Domain (Cháb and Žáček 1994).

### 2.2.1. Lithology and protolith ages

The core of the Desná Dome (Fig. 2) consists of orthogneisses, high-grade schists and amphibolite bodies of Neoproterozoic protolith ages (570–650 Ma, Kröner et al. 2000). The Devonian cover is composed of quartzite, metaconglomerate, metapelite and marble of Pragian to Tournaisian ages (Chlupáč 1989), and was intruded by Givetian volcanic rocks (Souček 1981; Patočka 1987) of arc and back-arc affinity (Janoušek et al. 2014). On the eastern side of the Desná Dome occurs a Culm sedimentary basin filled by Tournaisian to lowermost Pennsylvanian turbidite sequence (Hartley and Otava 2001). The Keprník Nappe (Fig. 2) is mainly formed by a Neoproterozoic orthogneiss (546–613 Ma, van Breemen et al. 1982; Kröner et al. 2000) and staurolite–sillimanite-bearing metapelites, calc-silicate intercalations, marble and quartzite. The hanging-wall Branná Group of presumably Devonian age is formed by low-grade metapelite, quartzite, porphyroid and marble. The westerly Velké Vrbno Unit (Fig. 2) consists of a Neoproterozoic tonalitic orthogneiss (Kröner et al. 2000), and a volcanosedimentary sequence composed of marble, graphitic schist, staurolite–kyanite-bearing micaschists and metavolcanic intercalations. The north-western part of the Silesian Domain was intruded by the Žulová granite Pluton, of which cooling is dated by the  $^{40}\text{Ar}$ – $^{39}\text{Ar}$  method on amphibole and biotite at  $292 \pm 3$  and  $290 \pm 3$  Ma, respectively (Maluski et al. 1995). These are undistinguishable from the emplacement ages recently determined as  $291 \pm 5$  Ma and  $292 \pm 4$  Ma (LA ICP-MS U–Pb dating on zircon: Laurent et al. this volume).

### 2.2.2. Variscan deformation and metamorphism

The oldest recognized structure is a pre-Variscan metamorphic fabric found only in the Desná Dome. The early Variscan foliation  $S_1$  is preserved as inclusion trails within garnet and staurolite and commonly also as the main matrix foliation, indicating that it was connected with the burial event (Štípská et al. 2006; Košuličová and Štípská 2007). The second deformation phase produced open to close asymmetric folds with subhorizontal NNE-trending hinges, west-dipping axial planes and axial planar crenulation cleavage  $S_2$ . Košuličová and Štípská (2007) argued that this stage started at the end of the burial, but continued during decompression, representing a major exhumation structure. The shallow west-dipping  $S_3$  foliation in the extensional zone at the western border



of the Keprník Dome is considered to be coeval with the intrusion of the Žulová Pluton (Cháb and Žáček 1994).

The Silesian Domain is affected by Barrovian type metamorphism, ranging from the chlorite zone in the east to the kyanite zone in the west (Souček 1978; Baratoux et al. 2005; Štípská et al. 2006; Košuličová and Štípská 2007 – Fig. 2). The Barrovian-type zonation is complicated by presence of eclogite boudins within the kyanite zone of the Velké Vrbno Unit (Žáček 1996; Štípská et al. 2006) and contrasting P–T paths of the micaschists that show prograde geothermal gradient of 16 °C/km in the westerly Velké Vrbno Unit and 29 °C/km in the Keprník Nappe and Desná Dome (Košuličová and Štípská 2007). Intrusion of the Žulová Pluton caused the overprinting of Barrovian metamorphism by HT–LP metamorphic assemblages with andalusite and cordierite that overgrow the S<sub>3</sub> foliation (Souček 1978;

**Fig. 2** Simplified geological map of the Silesian Domain (courtesy of J. Cháb) with metamorphic zones according to Košuličová and Štípská (2007). Locations of studied samples are also shown. Abbreviations for names of rock-forming minerals according to Kretz (1983).

Schulmann and Gayer 2000). The exact age of metamorphism in the Silesian Domain is presently unknown and existing  $^{40}\text{Ar}$ – $^{39}\text{Ar}$  radiometric measurements on muscovite, biotite and amphibole by Maluski et al. (1995) indicate cooling of the whole region between 300 and 323 Ma.

### 2.3. The Staré Město Belt and the Orlica–Śnieżnik Dome

#### 2.3.1. Lithology and protolith ages

The Staré Město Belt occurs to the west of the Velké Vrbno Unit and is formed by layered amphibolites and high-grade metasediments with Ordovician protoliths (Štípská et al. 2001). Variscan syntectonic granodiorite sill dated at ~339–344 Ma occurs to the west (Štípská et al. 2004). The Orlica–Śnieżnik Domain is dominated by granitoid orthogneisses with Cambro–Ordovician protolith ages that alternate with medium-grade metamorphosed Neoproterozoic to Cambro–Ordovician volcanosedimentary formation (Kröner et al. 2001; Jastrzębski et al. 2010; Mazur et al. 2012). Within the orthogneisses occur three belts of eclogite and omphacite granulite (Bakun-Czubarow 1998). The Cambro–Ordovician protolith age of the orthogneisses was a subject of several papers (e.g. Kröner et al. 2000, 2001 for review), while the controversial protolith ages for eclogites were recently discussed by Bröcker et al. (2010).

#### 2.3.2. Variscan metamorphism and deformation

The subhorizontal fabric in the Staré Město Belt was associated with *HT–MP* metamorphism (Kröner et al. 2000; Lexa et al. 2005; Jastrzębski et al. 2013). It was overprinted by west dipping foliation associated with the emplacement of a syntectonic granodiorite sill (Parry et al. 1997; Štípská et al. 2001). The dominant structure of the OSD is characterized by steep crustal-scale folding, where the synforms are formed by metamorphosed volcanosedimentary unit and cores of antiforms by vertically extruded high-pressure rocks (Don 1964; Štípská et al. 2012). The Variscan metamorphism and deformation in the area of the Staré Město was dated by Jastrzębski et al. (2013) who reported Late Devonian (CHIME) monazite, Lu–Hf garnet and U–Pb zircon ages. U–Th–Pb monazite dating of 335–315 Ma (Gordon et al. 2005) probably constrains fluid-driven recrystallization of monazite on retrograde P–T path. Cooling of the belt is dated by  $^{40}\text{Ar}$ – $^{39}\text{Ar}$  method on amphibole at 340–330 Ma (Maluski et al. 1995).

Several modern geochronological studies have indicated that the prograde metamorphism in the OSD

could have been of latest Devonian age (Klemd and Bröcker 1999; Gordon et al. 2005; Anczkiewicz et al. 2007; Bröcker et al. 2009, 2010). The amphibolite-facies reequilibration occurred probably during Early Carboniferous as shown by ~340 Ma U–Pb zircon ages (Turniak et al. 2000; Štípská et al. 2004; Lange et al. 2005) and U–Th–Pb monazite ages (Gordon et al. 2005). The cooling of the OSD is well constrained by numerous  $^{40}\text{Ar}$ – $^{39}\text{Ar}$  ages ranging from 340 to 335 Ma (Borkowska et al. 1990; Steltenpohl et al. 1993; Maluski et al. 1995; Marheine et al. 2002; Lange et al. 2002; Białek and Werner 2004; Schneider et al. 2006; Chopin et al. 2012). Nevertheless, there are some  $^{40}\text{Ar}$ – $^{39}\text{Ar}$  ages on muscovite and biotite and U–Th–Pb data on monazite of c. 315 Ma (Maluski et al. 1995; Gordon et al. 2005).

## 3. Analytical methods

Ages were determined using the conventional K–Ar method on muscovite and biotite, and the *in situ* U–Th–Pb dating on monazite by electron microprobe.

### 3.1. K–Ar dating of muscovite and biotite

The extracted biotite and muscovite were obtained from the 100–160  $\mu\text{m}$  sieve fraction using magnetic separation and, in two cases, by heavy liquids. The purity of micas was usually better than 98 %. In some samples from the chlorite–biotite zone, biotite was strongly retrogressed. Potassium was measured by flame photometry with a lithium internal standard, argon was extracted in a molybdenum crucible heated with a high-frequency current in a glass vacuum apparatus, and the radiogenic Ar was measured by isotope dilution ( $^{38}\text{Ar}$  as a tracer) using a MS 20 (A.E.I.) mass spectrometer at Institute de Physique de Globe, Strasbourg University. All samples were measured using the static method. The age calculation was done using constants recommended by Steiger and Jaeger (1977) and the  $2\sigma$  analytical uncertainty was calculated following Cox and Dalrymple (1967).

### 3.2. U–Th–Pb dating of monazite

Monazites were analysed in polished thin sections prepared for conventional electron microprobe analyses using a Cameca SX100 electron microprobe at “Laboratoire Magmas et Volcans” in Clermont-Ferrand, France. The analytical procedure followed Montel et al. (1996). Analytical conditions included an accelerating voltage of 15 kV and a beam current of 150 nA (for a detailed review of analytical conditions, counting times, standards used and X-ray lines and background offsets, see Bosse et al. 2009).

**Tab. 1** Result of K–Ar dating of muscovite and biotite

sample	metamorphic zone	mineral	K <sub>2</sub> O (wt.%)	% rad. <sup>40</sup> Ar / tot. <sup>40</sup> Ar	rad. <sup>40</sup> Ar (10 <sup>-11</sup> mol/g)	Age (± 2σ) in Ma
<i>Eastern margin of the Desná Dome</i>						
Mo 21	Chl–Bt	muscovite	4.432	97.3	241.0	343.0±5.1
Mo 212	Chl–Bt	muscovite	3.676	91.3	185.4	320.2±4.7
Mo-V	Chl–Bt	muscovite	6.901	96.3	309.2	287.1±4.3
Mo-H	Chl–Bt	muscovite	8.026	97.6	377.0	299.9±4.4
<i>Desná Dome and Keprník Nappe</i>						
Mo 40	staurolite	muscovite	6.139	95.3	255.0	267.6±3.9
Mo 41a	staurolite	biotite	7.500	96.3	308.5	265.2±3.9
Mo 237	staurolite	biotite	8.481	98.4	372.0	281.5±4.1
X 5	staurolite	biotite	6.456	89.2	267.2	266.8±4.0
X 11	garnet	muscovite	4.886	98.4	196.4	259.6±3.8
Mo 53	chloritoid	muscovite	6.823	94.5	319.8	299.3±4.5
MM 180	garnet	muscovite	7.767	97.7	367.5	301.9±4.4
MM 123	staurolite	muscovite	6.645	95.6	345.9	329.5±4.9
MM 175b	staurolite	biotite	6.455	80.4	262.7	262.6±4.0
MM 175b	staurolite	muscovite	8.414	93.1	374.2	285.2±4.3
MM 141	St–Sil	biotite	7.719	84.9	353.0	292.6±4.5
MM 141	St–Sil	muscovite	8.093	97.5	379.7	299.6±4.5
MM 88b	staurolite	biotite	6.914	88.5	316.3	292.7±4.4
MM 88b	staurolite	muscovite	7.777	84.9	338.5	279.5±4.4
MM 82	staurolite	muscovite	6.249	91.0	274.2	281.7±4.2
<i>Velké Vrbno Unit</i>						
S 523c	kyanite	biotite	7.646	93.9	401.1	331.9±5.1
S 485b	kyanite	muscovite	7.772	88.1	382.1	312.7±4.7
S 584b		amphibole	0.847	89.9	53.7	393.8±9.0
S 521d		amphibole	0.822	91.9	63.2	467.7±11.0

Individual ages were calculated from the U, Th and Pb concentrations according to the decay equation of Montel et al. (1996) assuming that non-radiogenic lead in monazite is negligible. The 2σ error on an individual measurement was calculated by propagating the uncertainties in U, Th and Pb determinations into the decay equation. The calculated 2σ age errors obtained from individual measurements are large, varying from ±10 to ±80 Ma. These 2σ errors on point analyses mainly depend on analytical counting times and on the U, Th and Pb contents in monazite (Montel et al. 1996). The resulting U–Th–Pb age population consists of the accumulated probability density functions for these individual ages.

The error can be considerably reduced assuming that the age population forms a consistent data set belonging to the same geological event (the same statistical population). Then the weighted average of the set was calculated using the least-squares method, yielding a single representative age with significantly smaller 2σ error. It is usually below 10 My for a set of 10–20 individual measurements. In order to further test the data quality for a given age population, classic isochron Th\* vs. Pb diagrams (Suzuki and Adachi 1991) were also used.

## 4. Geochronological results

The samples for K–Ar dating on muscovite and biotite and for U–Th–Pb dating on monazite were collected across all the metamorphic zones of the Silesian Domain, in the Keprník Nappe, the Desná Dome and the Velké Vrbno Unit (Fig. 2).

### 4.1. K–Ar dating results

The analytical results are presented geographically in three groups: (1) the Keprník Nappe and the western part of the Desná Dome, (2) the eastern margin of the Desná Dome and (3) the Velké Vrbno Unit (Tab. 1).

#### 4.1.1. The Keprník Nappe and the staurolite–garnet zones of the Desná Dome

Three groups of data can be distinguished: (1) a group of ~330 Ma represented only by the muscovite age of sample MM 123 from the staurolite zone in the western part of the Desná Dome; (2) three muscovite and one

biotite ages of ~300 Ma from samples located at least 1 km away from the thrust of the Keprník Nappe over the Desná Dome (Mo 53 chloritoid zone, MM 180 garnet zone, MM 141 staurolite zone) and (3) ages of ~260–280 Ma yielded by muscovite and biotite from the garnet or staurolite zones of the south-western Desná Dome (Mo 40, Mo 41a, X5, X11, Mo 237) and the western part of the Keprník Nappe (MM 175, MM 82, MM 88b) located in the staurolite zone.

#### 4.1.2. Biotite and chlorite zones of the eastern margin of the Desná Dome

Four muscovite fractions from the southern (Mo 21, Mo 212) and northern parts (Mo-V, Ho-H) of the Desná Dome are coming from the chlorite–biotite metamorphic zone. These samples yield apparent ages of  $320.2 \pm 4.7$ ,  $343 \pm 5.1$ ,  $287.1 \pm 4.3$ , and  $299.9 \pm 4.4$  Ma, respectively.

#### 4.1.3. Kyanite zone of the Velké Vrbno Unit

Two samples of kyanite micaschists (S523c, S485b) were collected. The biotite and muscovite give ages of  $332.0 \pm 5.1$  and  $313.0 \pm 4.7$  Ma, respectively.

### 4.2. Monazite U–Th–Pb (CHIME) dating results

In the metapelites of the Silesian Domain, monazite grains reach up to 80–30  $\mu\text{m}$  across. In the matrix, they are commonly arranged parallel with the main mineral fabric ( $S_2$ ) and rarely with the relics of earlier  $S_1$  fabric. In porphyroblasts, they are aligned along the  $S_1$  mineral inclusion trails (Figs 3–4). This indicates monazite growth synchronous with the development of the two main Variscan deformational fabrics ( $S_1$ ,  $S_2$ ). Ninety-seven analyses in monazite, included both in porphyroblasts and in matrix, were performed in 17 samples covering all units of the Silesian Domain. Back-scattered electron (BSE) images of dated monazites and their textural and mineralogical context are shown in Figs 3 and 4. Representative chemical compositions of monazite are presented in Tab. 2. Absolute U, Th and Pb contents, calculated individual ages and  $\text{Th}^*$  contents are discussed in Figs 5 to 7 and listed in Tab. 3. Statistical U–Th–Pb ages of monazites are presented in Fig. 8 and listed in Tab. 4.

One of the striking features of monazite analytical results is that the total of analysed elements ranges between 91.13 and 99.75 wt. % (Tab. 2). This may be due to the possible occurrence of volatile chemical components (such as S, As and OH) in monazites, and the lack of K and Zr measurements. The occurrence of volatiles and even some alkaline-earth metals in monazite is commonly

the result of late hydrothermal processes (e.g. Poitrasson et al. 1996, 2000), which may induce monazite-forming reactions (e.g. Catlos et al. 2002; Seydoux-Guillaume et al. 2002) and perturbations in U–Th–Pb ages (e.g. Cherniak et al. 2004; Gardés et al. 2006). Generally the  $\text{ThO}_2$  contents in monazite vary from < 1 to 30 wt. % although 4–12 wt. % is the most common range (Catlos et al. 2002 and references therein), and  $\text{UO}_2$  wt.% is lower than  $\text{ThO}_2$ . Our samples have low to moderate contents of  $\text{ThO}_2$  (1.3–10.3 %) and  $\text{UO}_2$  (0.16–1.47 %) (Fig. 5, Tab. 2), which brings rather significant errors on the calculated individual ages (Tab. 3). Figure 6 demonstrates that the calculated individual ages do not depend on the  $\text{Th}^*$  (i.e. measured Th plus Th equivalent of measured U) content of monazite. The  $2\sigma$  errors associated with each single age are inversely correlated with the  $\text{Th}^*$  content of monazite, which is consistent with the calculation algorithm. From these diagrams it appears that monazites included in porphyroblasts are slightly older than monazites located in the micaceous matrix, for both the Velké Vrbno Unit (Fig. 6a) and the Desná Dome with Keprník Nappe (Fig. 6b).

#### 4.2.1. The Desná Dome and Keprník Nappe

Monazites in garnet of four samples (Mo 43a, Mo 42b, Mo 44, Mo 41b) from the staurolite zone of the SW part of the Desná Dome give a range of ages from  $275 \pm 28$  to  $309 \pm 17$  Ma (Tab. 4). Monazite included in staurolite porphyroblasts was analyzed in five samples (Mo 45, Mo 43b, Mo 41b, MM 70b and MM 133) located close to the thrust of the Keprník Nappe over the Desná Dome. The details of microstructural positions of studied monazites and measured spots of samples Mo43b, Mo45 and Mo41b are shown in Fig. 3. The measured ages spread from  $252 \pm 22$  to  $288 \pm 14$  Ma. A monazite included in staurolite from a sample situated in the staurolite zone of the Keprník Nappe (MM 90) indicates an older age of  $317 \pm 21$  Ma. Matrix monazite ages from four samples (Mo 45, Mo 43b, Mo 41b and MM 133, Fig. 4a) are  $250 \pm 13$ ,  $268 \pm 8$ ,  $257 \pm 20$  and  $243 \pm 18$  Ma. The matrix monazites from samples MM142 and MM 71b situated in the sillimanite zone of the Keprník Nappe yield ages of  $290 \pm 17$  Ma and  $271 \pm 13$  Ma.

#### 4.2.2. The Velké Vrbno Unit

Monazite inclusions in garnet and staurolite porphyroblasts of the sample S573e define  $S_1$ – $S_2$  fabrics (Fig. 4c–d) and yield an age of  $321 \pm 8$  Ma, while the matrix monazite of the same sample gives  $314 \pm 12$  Ma. Only eight grains were found in the matrix of the kyanite–staurolite–garnet sample 627a (Fig. 4b) revealing an age of  $286 \pm 9$  Ma.

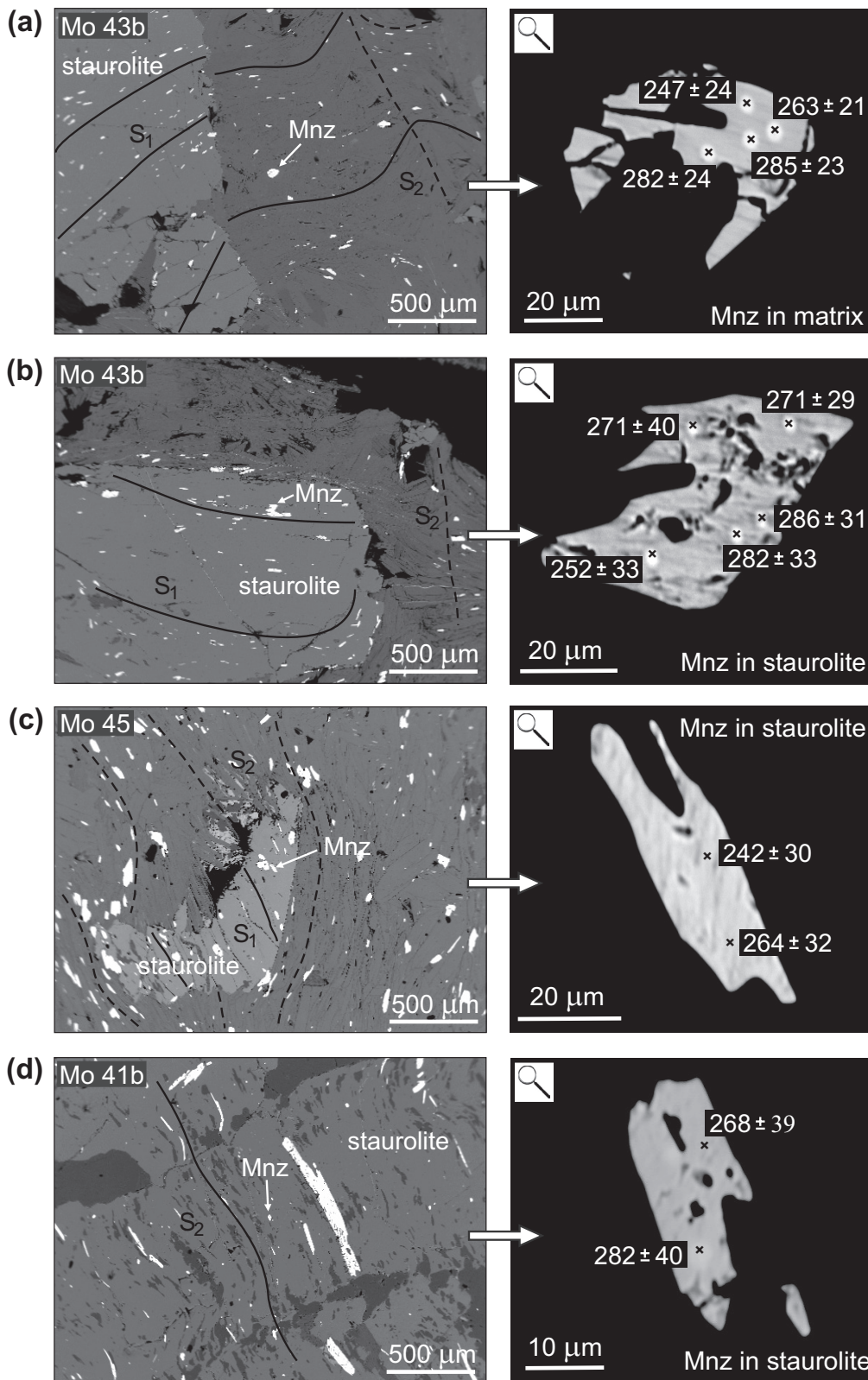


**Fig. 3** Back-scattered electron images of monazite grains (labelled by sample names) and their textural settings from the Desná Dome. Details show individual monazite grains with calculated ages and  $2\sigma$  errors, determined for analyzed points. **a** – Monazite crystal in the matrix parallel with the  $S_2$  fabric defined by quartz and micas. **b** – Monazite inclusion within a staurolite defining the  $S_1$  fabric. **c** – Monazite inclusion inside a staurolite parallel with matrix minerals. **d** – Monazite crystal in a staurolite growing in the  $S_2$  foliation.

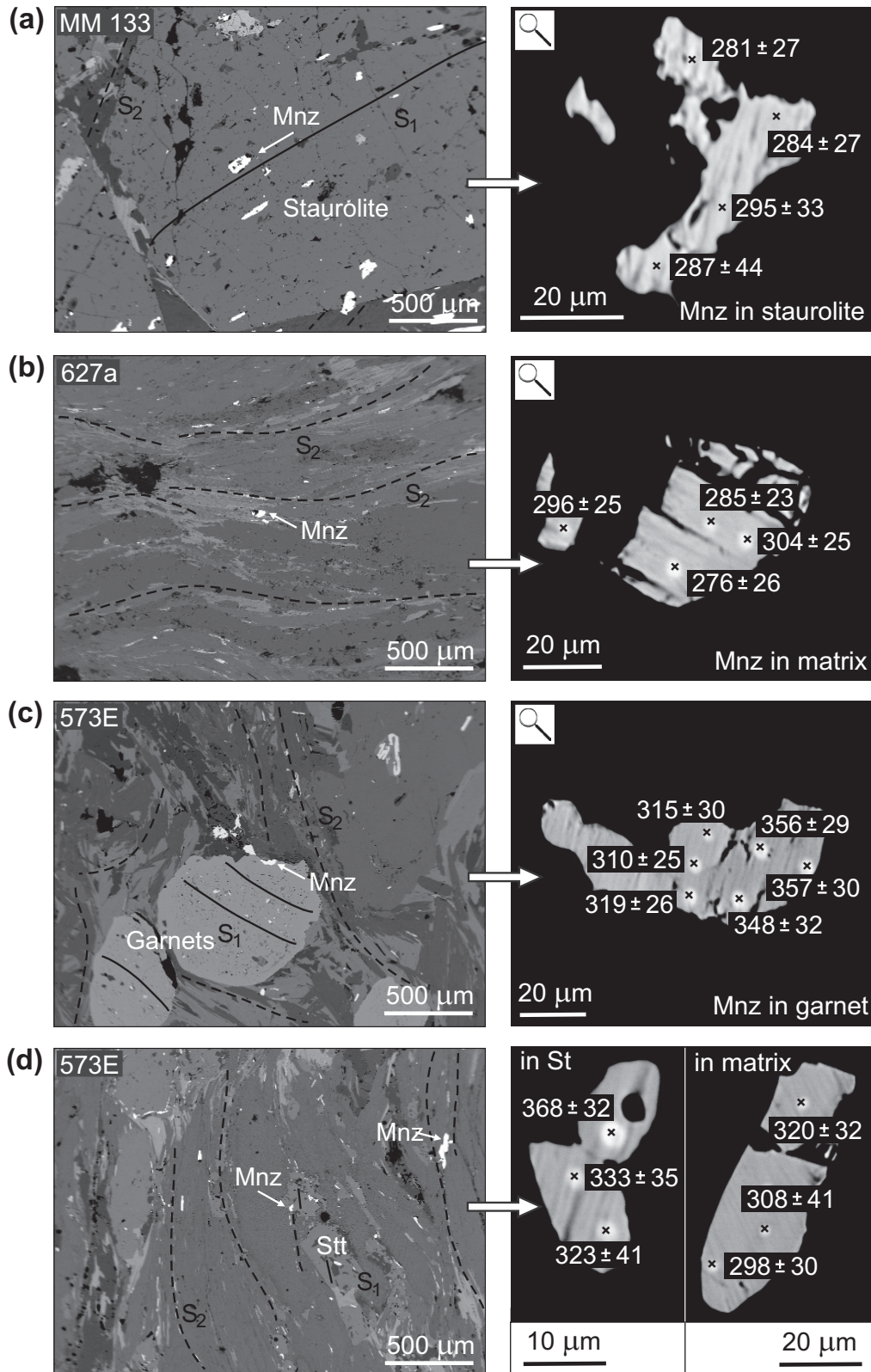


**Fig. 4** Back-scattered electron images of monazite grains (labelled by sample names) and their textural settings from the Kepník Nappe and the Velké Vrbno Unit. Details show individual monazite grains with calculated ages and  $2\sigma$  errors, determined for analyzed points. **a** – Monazite inclusion in staurolite (Kepník Nappe). **b** – Monazite aligned with S<sub>2</sub> fabric, defined also by micas and quartz (Velké Vrbno Unit). **c** – Monazite inclusion within garnet located at the rim and showing orientation of S<sub>1</sub> fabric (Velké Vrbno Unit). **d** – Monazite grain at the staurolite rim is parallel with the external fabric, including elongated monazite crystal (Velké Vrbno Unit).

Tab. 2 Monazite chemical compositions

sample	point	position	UO <sub>2</sub>	PbO	ThO <sub>2</sub>	CaO	P <sub>2</sub> O <sub>5</sub>	Y <sub>2</sub> O <sub>3</sub>	SiO <sub>2</sub>	La <sub>2</sub> O <sub>3</sub>	Ce <sub>2</sub> O <sub>3</sub>	Pr <sub>2</sub> O <sub>3</sub>	Nd <sub>2</sub> O <sub>3</sub>	SmO	Gd <sub>2</sub> O <sub>3</sub>	Total
<i>Desná Dome and Keprník Nappe</i>																
MM 142	7	matrix	0.643	0.055	2.291	0.648	28.836	1.714	0.439	13.309	28.757	3.005	12.715	2.156	1.600	96.168
	8	matrix	0.992	0.074	2.798	0.824	28.891	1.749	0.308	13.051	28.307	3.022	12.288	2.057	1.554	95.915
	9	matrix	0.606	0.061	2.469	0.620	28.797	1.553	0.233	13.477	28.709	3.022	12.520	2.161	1.545	95.773
	10	matrix	0.826	0.065	2.558	0.674	28.506	1.016	0.160	14.192	29.206	3.064	11.842	2.016	1.619	95.744
	11	matrix	0.698	0.054	2.593	0.611	28.108	0.845	0.913	14.394	28.928	3.037	11.694	1.903	1.405	95.183
	MM 133	13	matrix	0.616	0.085	5.815	1.142	28.376	0.282	0.272	13.794	28.346	2.736	11.236	2.011	1.557
14		matrix	0.474	0.046	3.303	0.693	28.917	0.364	0.137	14.486	29.891	2.927	11.457	1.979	1.515	96.189
15		matrix	0.430	0.058	4.492	0.819	28.477	0.364	0.246	14.068	29.318	2.890	11.470	1.997	1.528	96.157
18		in staurolite	0.418	0.088	6.042	1.100	25.990	0.624	2.227	12.434	26.064	2.639	10.489	1.815	1.494	91.424
19		in staurolite	0.381	0.089	6.175	1.145	25.892	0.604	1.361	12.373	26.329	2.658	10.651	1.872	1.511	91.041
20		in staurolite	0.441	0.075	4.597	0.979	27.157	0.574	1.029	13.081	27.315	2.826	11.068	1.837	1.526	92.505
MM 71b	21	in staurolite	0.382	0.053	3.088	0.736	26.105	0.353	6.743	12.767	26.587	2.673	10.643	1.802	1.422	93.354
	22	matrix	0.580	0.101	6.684	1.312	28.192	0.810	0.389	13.209	27.375	2.803	10.697	1.949	1.667	95.768
	23	matrix	0.577	0.102	7.100	1.321	27.063	0.828	2.022	12.586	26.184	2.622	10.031	1.837	1.564	93.837
	24	matrix	0.678	0.088	5.579	1.080	28.681	0.902	0.272	13.296	27.872	2.926	11.187	2.054	1.857	96.472
	25	matrix	0.533	0.082	5.387	0.984	27.801	0.825	0.817	13.192	27.446	2.880	11.175	1.920	1.749	94.791
Mo 45	27	in staurolite	0.587	0.067	4.597	0.935	28.231	0.263	0.466	12.203	28.974	2.975	11.996	2.004	1.387	94.685
	28	in staurolite	0.552	0.067	4.157	0.907	27.819	0.278	1.393	12.078	28.264	2.816	11.636	2.075	1.434	93.476
	29	matrix	0.819	0.078	3.757	0.805	28.490	0.314	0.193	12.001	29.960	3.019	12.231	1.946	1.632	95.245
	30	matrix	0.736	0.053	3.026	0.662	28.642	0.358	0.148	12.570	30.760	2.984	12.253	2.048	1.684	95.924
	31	matrix	0.637	0.068	4.827	1.007	28.703	0.260	0.175	12.709	29.296	2.884	11.918	2.165	1.543	96.192
	32	matrix	0.642	0.075	5.069	1.037	28.651	0.277	0.201	12.550	28.929	3.057	11.871	2.113	1.535	96.007
	33	matrix	0.768	0.088	5.744	1.221	28.745	0.392	0.210	12.611	28.081	2.873	11.500	2.082	1.784	96.099
Mo 43b	1	matrix	1.167	0.102	4.748	1.104	28.981	0.443	0.165	11.210	26.819	3.326	14.183	2.712	1.747	96.707
	2	matrix	1.191	0.108	5.035	1.175	28.758	0.431	0.169	11.047	26.576	3.249	14.365	2.766	1.730	96.600
	3	matrix	0.885	0.108	6.756	1.249	28.390	0.461	0.255	10.967	26.601	3.196	13.693	2.668	1.762	96.991
	4	matrix	1.078	0.087	4.844	1.069	28.664	0.395	0.182	11.178	26.865	3.268	14.212	2.713	1.705	96.260
	5	in staurolite	0.791	0.066	3.970	0.733	27.363	0.340	0.762	11.893	27.876	3.214	13.924	2.582	1.554	95.068
	6	in staurolite	0.773	0.062	3.145	0.718	28.949	0.337	0.210	11.641	27.688	3.363	14.210	2.649	1.568	95.313
	7	in staurolite	0.756	0.064	3.533	0.824	28.946	0.339	2.073	10.836	25.948	3.163	13.419	2.496	1.475	93.872
	8	matrix	0.824	0.096	6.611	1.347	28.577	0.439	0.285	10.761	26.204	3.224	13.524	2.668	1.692	96.252
	9	matrix	0.473	0.075	5.263	1.087	28.678	0.226	0.235	11.052	28.695	3.127	13.554	2.461	1.224	96.150
	10	matrix	0.696	0.127	8.483	1.515	28.179	0.660	0.483	9.839	26.136	3.023	12.820	2.591	2.105	96.657
	11	matrix	0.936	0.155	10.311	1.945	28.078	0.721	0.492	9.296	24.189	2.818	12.254	2.552	2.077	95.824
Mo 41b	12	in staurolite	1.021	0.062	2.520	0.834	28.988	0.960	0.101	11.820	29.576	3.110	12.641	2.408	1.829	95.870
	13	in staurolite	1.006	0.071	2.671	0.719	29.136	1.005	0.073	12.036	29.402	3.028	12.540	2.400	1.924	96.011
	14	in staurolite	1.035	0.076	2.936	0.916	28.962	0.916	0.120	11.576	29.250	3.084	12.746	2.310	1.859	95.786
	15	in staurolite	0.822	0.055	2.109	0.554	28.543	1.046	0.079	11.445	29.775	3.193	13.348	2.492	1.996	95.457
	16	in staurolite	1.264	0.079	2.718	0.904	29.201	1.314	0.116	10.990	28.653	3.063	12.929	2.565	1.966	95.762
	48	in garnet	0.272	0.059	4.066	0.830	27.972	1.133	0.216	13.835	27.917	2.934	11.951	2.070	1.518	94.773
	49	in garnet	0.338	0.057	3.934	0.806	28.710	1.255	0.124	13.732	27.551	2.918	12.130	2.260	1.666	95.481
	21	in staurolite	0.424	0.069	4.711	0.960	30.530	1.311	0.175	12.506	26.815	2.943	13.816	2.483	2.101	98.844
	23	in staurolite	0.379	0.084	5.043	1.019	30.186	1.076	0.195	12.717	26.655	3.035	13.622	2.429	1.913	98.353
	24	in staurolite	0.312	0.044	3.194	0.677	30.367	1.158	0.109	13.008	28.071	3.114	13.893	2.461	2.181	98.589
	25	in staurolite	0.372	0.054	3.458	0.779	30.440	1.245	0.105	12.855	27.316	2.923	13.869	2.544	2.219	98.179
52	matrix	0.302	0.054	3.609	0.708	29.576	1.130	0.188	13.725	27.541	2.854	12.317	2.273	1.705	95.982	
53	matrix	0.347	0.059	4.228	0.874	29.439	1.267	0.135	13.388	27.314	2.859	12.275	2.205	1.672	96.062	
54	matrix	0.324	0.052	3.876	0.817	29.389	1.250	0.137	13.772	27.620	2.892	12.282	2.296	1.651	96.358	
55	matrix	0.318	0.046	3.483	0.747	29.423	1.278	0.109	14.024	27.780	2.957	12.470	2.177	1.642	96.454	

Tab. 2 continued

sample	point	position	UO <sub>2</sub>	PbO	ThO <sub>2</sub>	CaO	P <sub>2</sub> O <sub>5</sub>	Y <sub>2</sub> O <sub>3</sub>	SiO <sub>2</sub>	La <sub>2</sub> O <sub>3</sub>	Ce <sub>2</sub> O <sub>3</sub>	Pr <sub>2</sub> O <sub>3</sub>	Nd <sub>2</sub> O <sub>3</sub>	SmO	Gd <sub>2</sub> O <sub>3</sub>	Total	
MM 70b	1	in staurolite	1.475	0.142	5.447	1.493	31.540	1.726	2.526	12.642	24.969	2.613	10.916	1.681	1.677	98.847	
	3	in staurolite	1.402	0.106	5.254	1.518	29.991	1.474	3.549	12.911	23.840	2.409	10.279	1.677	1.601	96.011	
	5	in staurolite	0.305	0.062	4.139	0.651	30.504	1.886	0.462	14.046	28.291	2.854	12.087	1.699	1.538	98.524	
MM 90	7	in staurolite	0.462	0.066	3.235	0.625	31.398	1.351	0.195	14.106	29.285	2.928	12.119	1.636	1.350	98.756	
	9	in staurolite	0.381	0.036	1.299	0.332	31.176	1.398	0.079	14.183	30.282	3.193	12.703	1.896	1.434	98.392	
	12	in staurolite	0.346	0.032	1.342	0.304	30.667	1.233	0.068	14.825	30.768	3.188	12.547	1.810	1.343	98.473	
	13	in staurolite	0.357	0.036	1.345	0.323	30.857	1.448	0.083	14.723	30.271	3.097	12.864	1.954	1.619	98.977	
	17	in staurolite	0.477	0.081	4.313	0.858	30.229	1.317	0.257	13.597	28.722	2.844	11.713	1.585	1.369	97.362	
Mo 43a	11	in garnet	0.543	0.054	2.147	0.719	30.601	0.970	0.109	12.301	28.816	3.471	14.407	2.477	1.749	98.364	
	12	in garnet	0.533	0.051	2.140	0.557	30.628	1.406	0.098	11.077	27.658	3.451	15.469	2.931	2.068	98.067	
	13	in garnet	0.577	0.052	1.928	0.555	30.486	1.309	0.092	11.485	28.153	3.421	15.497	2.769	1.997	98.321	
	14	in garnet	1.276	0.094	3.099	0.925	30.023	1.356	0.175	11.232	26.936	3.242	14.248	2.522	2.040	97.168	
	15	in garnet	0.704	0.052	2.055	0.568	30.420	0.683	0.101	11.640	28.663	3.345	16.073	2.790	1.826	98.920	
	16	in garnet	0.825	0.069	2.204	0.648	30.864	1.990	0.141	11.078	27.302	3.421	15.112	2.790	2.057	98.501	
Mo 42b	17	in staurolite	0.165	0.030	1.666	0.388	30.170	1.290	0.047	13.616	24.108	3.773	16.616	3.198	2.732	97.799	
	18	in staurolite	0.304	0.038	1.860	0.460	30.651	1.502	0.062	13.245	23.318	3.729	16.643	3.092	3.103	98.007	
	19	in staurolite	0.241	0.039	2.609	0.574	30.575	1.466	0.081	12.892	23.049	3.686	16.614	3.428	3.190	98.444	
	20	in staurolite	0.171	0.032	1.941	0.462	31.041	1.289	0.071	13.289	23.951	3.736	16.509	3.177	2.773	98.442	
Mo 44	15	in staurolite	0.757	0.150	9.537	1.791	30.715	1.783	0.413	11.261	25.065	2.687	11.411	2.148	1.931	99.649	
<i>Velké Vrbno Unit</i>																	
627a	18	matrix	0.622	0.132	7.712	1.380	28.465	0.387	0.462	15.866	27.084	2.535	9.625	1.903	1.406	97.579	
	19	matrix	0.957	0.107	5.167	1.192	28.896	0.770	0.150	15.269	28.349	2.774	10.294	1.649	1.239	96.813	
	20	matrix	0.643	0.110	6.975	1.319	28.534	0.375	0.319	15.896	27.409	2.405	9.591	1.885	1.515	96.976	
	22	matrix	1.096	0.103	4.636	1.180	29.363	0.808	0.062	15.303	28.592	2.808	10.051	1.585	1.143	96.730	
	23	matrix	0.646	0.090	5.624	1.153	28.009	0.380	0.246	17.021	28.109	2.654	9.344	1.499	0.958	95.733	
	24	matrix	0.603	0.076	4.975	0.975	28.554	0.211	0.231	15.647	28.824	2.787	10.472	1.533	1.234	96.122	
	25	matrix	0.938	0.089	4.747	1.115	28.490	0.047	0.145	15.206	29.631	2.964	10.602	1.410	0.649	96.033	
	26	matrix	0.427	0.041	2.943	0.683	27.042	0.314	0.120	15.744	30.441	2.915	10.837	1.481	1.113	94.101	
	573E	28	matrix	0.553	0.072	3.625	0.916	28.804	2.351	0.073	13.734	28.550	2.779	10.356	1.597	1.541	94.951
		29	matrix	0.597	0.078	3.810	0.932	29.015	2.158	0.077	14.504	28.754	2.748	10.093	1.498	1.241	95.505
30		matrix	0.649	0.115	6.865	1.301	28.513	0.640	0.319	14.186	27.393	2.551	9.959	1.853	2.039	96.383	
31		matrix	0.561	0.086	5.002	1.167	28.399	2.075	0.188	14.236	27.903	2.675	9.926	1.572	1.545	95.335	
32		matrix	0.479	0.064	3.301	0.905	28.587	2.137	0.126	14.600	28.675	2.749	10.020	1.521	1.562	94.726	
33		matrix	0.696	0.089	4.300	1.083	28.816	2.078	0.101	13.844	28.458	2.662	10.278	1.518	1.459	95.382	
34		matrix	0.677	0.107	5.174	1.258	28.614	2.390	0.212	13.640	27.624	2.559	9.988	1.652	1.664	95.559	
27		in garnet	0.664	0.080	3.721	0.930	29.001	2.177	0.086	14.012	28.887	2.758	10.425	1.520	1.536	95.797	
35		in garnet	1.139	0.108	4.238	1.100	28.843	1.138	0.077	15.008	28.867	2.606	9.761	1.522	1.399	95.806	
36		in garnet	0.736	0.098	4.223	1.181	28.903	2.503	0.098	13.848	28.236	2.712	9.934	1.620	1.646	95.738	
37		in garnet	0.857	0.107	4.240	1.173	29.157	2.365	0.079	14.020	28.094	2.563	9.921	1.579	1.595	95.750	
38		in garnet	0.704	0.111	5.034	1.314	29.015	2.555	0.122	13.712	27.436	2.619	9.682	1.582	1.396	95.282	
39		in garnet	0.739	0.093	4.517	1.156	29.141	2.095	0.152	14.606	28.777	2.619	9.326	1.422	1.429	96.072	
40		in garnet	1.305	0.112	4.265	1.115	28.882	1.295	0.094	14.440	28.560	2.555	9.973	1.608	1.497	95.701	
41		in staurolite	0.406	0.067	3.548	0.792	28.105	2.089	0.246	13.829	28.885	2.872	10.927	1.819	1.433	95.018	
42		in staurolite	0.520	0.084	4.240	0.986	28.392	2.253	0.158	13.703	28.046	2.835	10.629	1.860	1.417	95.123	
43		in staurolite	0.563	0.104	4.826	1.115	28.204	2.161	0.197	13.613	27.975	2.909	10.367	1.712	1.340	95.086	
44	in staurolite	0.603	0.084	4.062	0.984	28.800	2.053	0.066	14.088	28.698	2.779	10.107	1.510	1.486	95.320		
45	in staurolite	0.605	0.142	8.910	1.547	28.399	0.071	0.524	15.088	27.699	2.431	9.624	1.504	0.735	97.279		
46	in staurolite	0.543	0.085	5.297	1.122	28.658	0.401	0.248	14.839	29.520	2.964	10.472	1.478	0.985	96.612		
47	in staurolite	0.713	0.111	6.656	1.382	28.674	0.396	0.272	13.969	28.723	2.747	10.385	1.532	1.021	96.581		

Tab. 3 Monazite U–Th–Pb geochronological results

sample	point	location	Th (ppm)	$\sigma$	U (ppm)	$\sigma$	Pb (ppm)	$\sigma$	DL	Age	$\sigma$	Th* (ppm)
<i>Desná Dome and Keprník Nappe</i>												
MM 142	7	matrix	20130	436	5670	178	510	64	114	295	44	37660
	8	matrix	24590	469	8750	191	690	66	116	290	33	51635
	9	matrix	21700	446	5340	178	570	64	114	325	44	38236
	10	matrix	22480	451	7290	184	600	65	115	290	37	45013
	11	matrix	22790	453	6150	180	500	64	115	261	39	41770
MM 133	13	matrix	51100	605	5430	180	790	67	117	257	26	67854
	14	matrix	29030	490	4180	174	430	64	116	226	39	41906
	15	matrix	39480	548	3790	173	540	64	115	233	32	51159
	18	in staurolite	53100	612	3690	171	820	66	114	281	27	64500
	19	in staurolite	54270	616	3360	169	830	65	112	284	27	64652
MM 71b	20	in staurolite	40400	548	3890	170	700	65	115	295	33	52427
	21	in staurolite	27140	477	3370	167	490	64	114	287	44	37555
	22	matrix	58740	640	5110	178	940	68	117	278	24	74524
	23	matrix	62400	654	5090	178	950	68	116	269	23	78115
	24	matrix	49030	594	5980	180	820	67	117	267	26	67491
Mo 45	25	matrix	47340	588	4700	176	760	67	116	271	28	61852
	27	in staurolite	40400	553	5180	177	620	65	115	242	30	56370
	28	in staurolite	36530	533	4870	176	620	64	114	264	32	51562
	29	matrix	33020	514	7220	185	720	66	116	285	31	55330
	30	matrix	26590	477	6490	182	490	64	116	230	35	46586
Mo 43b	31	matrix	42420	562	5610	179	630	66	116	232	28	59706
	32	matrix	44550	572	5660	180	700	66	117	249	28	62006
	33	matrix	50480	601	6770	184	820	68	118	252	25	71363
	1	matrix	41730	562	10280	198	950	68	117	282	24	73491
	2	matrix	44250	572	10500	198	1000	68	116	285	23	76696
	3	matrix	59370	643	7800	190	1000	69	117	263	21	83444
	4	matrix	42570	565	9500	194	810	67	117	247	24	71866
	5	in staurolite	34890	525	6980	184	610	64	113	237	29	56404
	6	in staurolite	27640	484	6810	184	580	62	110	261	33	48656
	7	in staurolite	31050	506	6670	185	590	59	104	250	30	51622
	8	matrix	58100	638	7270	188	890	67	116	244	22	80516
	9	matrix	46250	583	4170	175	700	66	116	262	29	59120
	10	matrix	74550	705	6130	183	1180	70	118	278	20	93485
	11	matrix	90610	769	8250	192	1440	73	119	273	17	116087
	12	in staurolite	22150	450	9000	191	580	65	116	252	33	49912
13	in staurolite	23470	457	8870	191	660	66	116	282	33	50875	
14	in staurolite	25800	470	9120	191	710	65	115	286	31	53983	
15	in staurolite	18530	427	7250	185	510	64	114	271	40	40916	
16	in staurolite	23890	461	11150	199	730	65	115	271	29	58319	
Mo 41b	21	in garnet	41400	562	3730	174	640	67	118	267	33	52915
	23	in garnet	44320	574	3340	171	780	67	117	316	33	54658
	24	in staurolite	28070	487	2750	169	410	65	118	248	46	36551
	25	in staurolite	30390	500	3280	171	500	66	118	272	43	40518
	48	in staurolite	35730	531	2400	168	550	65	117	282	40	43145
	49	in staurolite	34570	521	2980	170	530	66	117	268	39	43770
	52	matrix	31720	510	2660	170	500	64	115	276	42	39936
	53	matrix	37160	539	3060	171	550	64	115	261	36	46604
	54	matrix	34060	521	2850	170	480	64	115	248	36	42849
55	matrix	30610	511	2810	169	430	63	111	242	33	39273	

Tab. 3 continued

sample	point	location	Th (ppm)	$\sigma$	U (ppm)	$\sigma$	Pb (ppm)	$\sigma$	DL	Age	$\sigma$	Th* (ppm)	
MM 70b	1	in staurolite	47870	588	13000	205	1320	68	111	326	21	88129	
	3	in staurolite	46170	580	12350	198	980	67	114	254	20	84269	
	5	in staurolite	36370	531	2690	169	580	65	115	287	38	44683	
MM 90	7	in staurolite	28430	485	4070	173	610	65	115	326	42	41034	
	9	in staurolite	11420	372	3360	170	330	63	115	329	75	21827	
	12	in staurolite	11790	370	3050	169	300	65	118	308	78	21226	
	13	in staurolite	11820	377	3140	169	330	65	118	334	79	21548	
	17	in staurolite	37900	536	4210	172	750	67	117	324	35	50936	
Mo 43a	11	in garnet	18870	426	4790	175	500	64	114	323	50	33701	
	12	in garnet	18810	429	4700	175	470	64	115	308	50	33351	
	13	in garnet	16940	416	5090	177	480	65	117	319	52	32697	
	14	in garnet	27230	480	11250	198	870	67	116	304	28	62029	
	15	in garnet	18060	424	6200	181	480	66	118	280	45	37213	
	16	in garnet	19370	432	7280	185	640	65	115	331	41	41921	
Mo 42b	17	in staurolite	14640	400	1450	163	280	64	116	323	88	19130	
	18	in staurolite	16350	412	2680	169	350	65	118	312	69	24643	
	19	in staurolite	22930	459	2130	167	360	64	116	269	56	29506	
	20	in staurolite	17060	418	1510	163	300	64	117	305	78	21731	
Mo 44	15	in staurolite	83810	745	6680	186	1390	73	120	294	19	104462	
<i>Velké Vrbno Unit</i>													
627a	18	matrix	67770	676	5490	181	1230	71	119	320	23	84766	
	19	matrix	45410	576	8440	189	990	69	118	304	25	71517	
	20	matrix	61300	649	5670	181	1020	70	119	285	23	78821	
	22	matrix	40740	552	9670	193	960	68	116	296	25	70638	
	23	matrix	49420	594	5700	179	840	67	116	276	26	67025	
	24	matrix	43720	565	5310	178	710	66	116	260	28	60106	
	25	matrix	41720	557	8270	188	830	67	117	271	26	67256	
	26	matrix	25860	467	3760	170	380	64	115	223	43	37440	
	573E	27	matrix	32700	509	5850	181	740	66	115	319	34	50810
		28	matrix	31860	505	4880	177	670	66	117	313	37	46962
		29	matrix	33480	515	5260	178	720	66	116	317	35	49762
		30	matrix	60330	644	5720	181	1070	69	117	303	24	78022
		31	matrix	43960	570	4940	177	800	67	117	298	30	59236
		32	matrix	29010	488	4220	174	590	66	117	308	41	42066
33		matrix	37790	540	6130	181	830	68	117	320	32	56768	
34		in garnet	45470	581	5970	183	990	69	119	340	29	63972	
35		in garnet	37240	536	10040	195	1000	68	117	319	26	68321	
36		in garnet	37110	533	6490	182	910	68	117	348	32	57232	
37		in garnet	37260	533	7560	187	990	68	116	357	30	60711	
38	in garnet	44240	572	6200	183	1030	68	116	356	29	63471		
39	in garnet	39700	546	6510	182	860	67	117	315	30	59849		
40	in garnet	37480	537	11500	200	1040	69	117	310	25	73063		
41	in staurolite	31180	503	3580	171	620	65	115	323	41	42265		
42	in staurolite	37260	535	4590	176	780	66	116	333	35	51480		
43	in staurolite	42410	562	4960	177	970	68	117	368	32	57805		
44	in staurolite	35700	526	5310	177	780	67	117	328	34	52146		
45	in staurolite	78300	718	5330	180	1320	72	119	308	20	94790		
46	in staurolite	46550	582	4790	178	790	67	116	284	29	61351		
47	in staurolite	58490	638	6290	184	1030	69	117	291	23	77933		

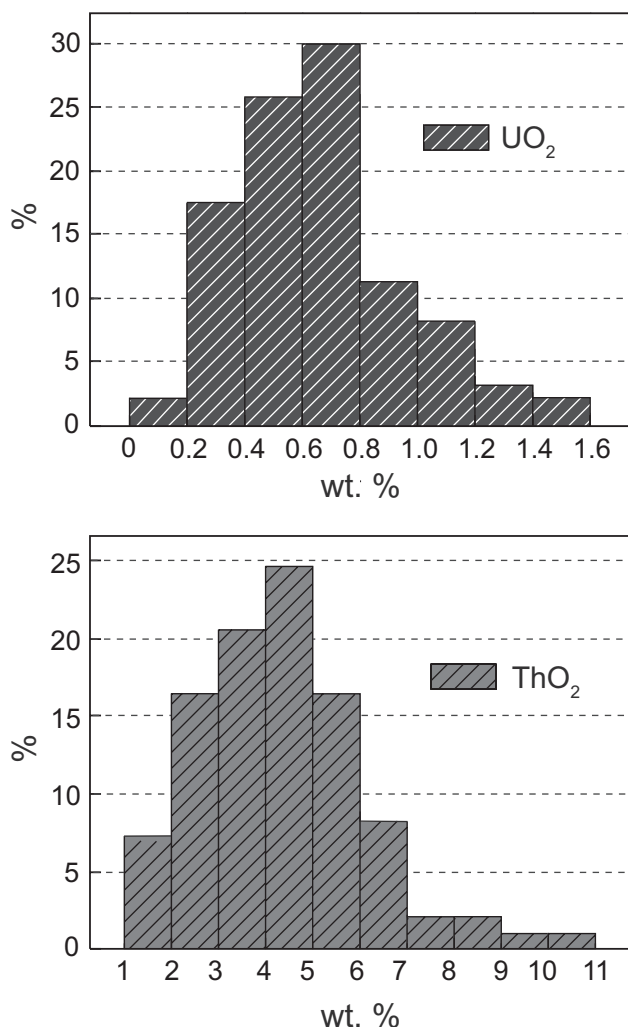


Fig. 5 Histograms of ThO<sub>2</sub> and UO<sub>2</sub> contents (wt. %) in all electron-microprobe analyses of monazite.

#### 4.2.3. Statistical U–Th–Pb monazite dating

Conventional Th\* vs. Pb isochron diagrams drawn for monazites located in matrix and included in porphyroblasts, for both the Velké Vrbno Unit (Fig. 7a) and the Desná Dome with Keprník Nappe (Fig. 7b), highlight that each monazite type belongs to a single population. The isochron line suggests slight age differences between distinct monazite populations. As a consequence, an extensive set of analyses is needed to reduce the uncertainties using a statistical method (Montel et al. 1996).

Statistical monazite U–Th–Pb ages results from the Silesian Domain are summarized in Tab. 4 and probability density functions for the Desná Dome and the Keprník Nappe with the Velké Vrbno Unit are illustrated in Fig. 8. The diagrams evidence that matrix monazites display younger ages than those enclosed in porphyroblasts. The narrow peaks of average ages and their corresponding errors were obtained statistically, assuming the consistency

of the samples (Montel et al. 1996). In the Velké Vrbno Unit the matrix and inclusion monazites yield  $297 \pm 7$  Ma and  $322 \pm 8$  Ma U–Th–Pb ages, respectively (Fig. 8a). In the Desná Dome and the Keprník Nappe the matrix and inclusion monazites indicate U–Th–Pb ages of  $263 \pm 5$  and  $283 \pm 6$  Ma, respectively (Fig. 8d).

## 5. Discussion and conclusions

The main goal of this work is to discuss the fact that the K–Ar ages of the Silesian Domain are significantly younger compared to the rest of the eastern margin of the Variscan front. The second important question is the possibility of preservation of older ages in the Velké Vrbno Unit and easternmost lower grade contact between the Silesian Domain and the Culm basin, supposing that the younger ages of the central part of the Silesian Domain may be thermally rejuvenated by the Žulová Pluton. The U–Th–Pb study on monazite from the OSD domain (Gordon et al. 2005) gave similar age range (340–330 Ma) as the <sup>40</sup>Ar–<sup>39</sup>Ar method (Schneider et al. 2006). Therefore, the question arises as whether the monazites preserved as inclusions in prograde mineral porphyroblasts in the Silesian Domain may yield similar Early Carboniferous ages, while the matrix monazites may record exhumation and/or cooling of the whole Silesian Domain. All these questions are addressed by this

Tab. 4 Weighted averages of individual monazite ages given in Tab. 3

sample	position	# of analyses	Th–U–Pb age (Ma)	2σ error (Ma)
<i>Desná Dome</i>				
Mo 45	in staurolite	2	252	± 22
Mo 45	matrix	5	250	± 13
Mo 43b	matrix	8	268	± 8
Mo 43b	in staurolite	8	263	± 11
Mo 43a	in garnet	6	309	± 17
Mo 41b	in staurolite	4	281	± 19
Mo 41b	in garnet	2	275	± 28
Mo 41b	matrix	4	257	± 20
Mo 42b	in garnet	4	296	± 35
Mo 44	in garnet	1	294	± 19
<i>Keprník Nappe</i>				
MM 142	matrix	5	290	± 17
MM 133	matrix	3	243	± 18
MM 133	in staurolite	4	286	± 15
MM 71b	matrix	4	271	± 13
MM 70b	in staurolite	3	288	± 14
MM 90	in staurolite	5	317	± 21
<i>Velké Vrbno Unit</i>				
627a	matrix	8	286	± 9
573E	in g/st	14	321	± 8
573E	matrix	7	314	± 12

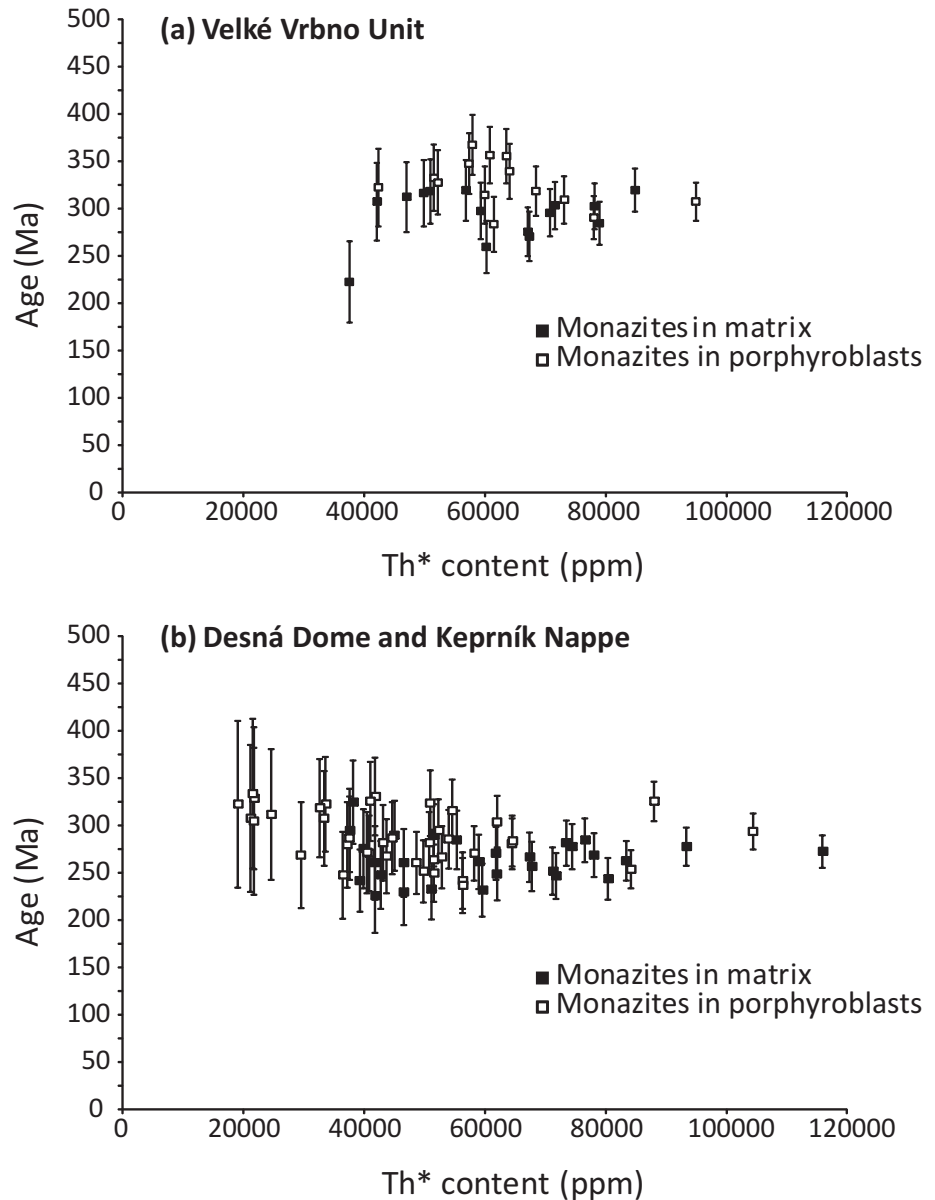


**Fig. 6** Plot of Th\* (ppm; measured Th plus Th equivalent of measured U *sensu* Suzuki and Adachi 1991) vs. calculated individual ages (Ma;  $2\sigma$  uncertainties) for all analysed monazites in both the Velké Vrbno Unit (a) and the Keprník Nappe with the Desná Dome (b). Black squares correspond to analyses of matrix monazites and white squares to monazite grains included in porphyroblasts.

study and a new model of cooling and tectonic history of this important part of the Variscan front is proposed.

### 5.1. Significance of K–Ar and U–Th–Pb ages

Generally accepted values for closure temperature of K–Ar in biotite and muscovite are *c.* 300 °C and 350–400 °C, respectively. However, the closure temperature of muscovite is not known exactly (McDougall and Harrison 1988) and for example Villa (1997) suggested that it could be higher, *c.* 400–450 °C. Geological estimates for the closure temperature of Pb in monazite vary from 530 °C to 750 °C (Köppel et al. 1980; Black et al. 1984; Copeland et al. 1988; Parrish 1990; Suzuki et al. 1994). On a crystal-chemical basis, Dahl (1997) contended that the closure temperature of Pb in monazite is higher than

750 °C and recent measurements of Pb diffusion in monazite led Cherniak et al. (2004) and Gardés et al. (2007) to the conclusion that monazite has a closure temperature greater than 800 °C. According to the theory of cooling ages (Dodson 1979), the metamorphic terrains should therefore yield older U–Th–Pb monazite ages than K–Ar muscovite and biotite ages. However, the data obtained on matrix monazite and on muscovite and biotite in the three areas of the Silesian Domain reveal the opposite. Monazite grains in the studied Silesian metapelites display alteration features (irregular shapes, rough surfaces and fractures, Fig. 3) that could be related to significant fluid-related dissolution processes. Experimental studies (Seydoux-Guillaume et al. 2002) have demonstrated that the U–Th–Pb system in monazite is sensitive to fluid-rock interactions. Accordingly, we propose that this process

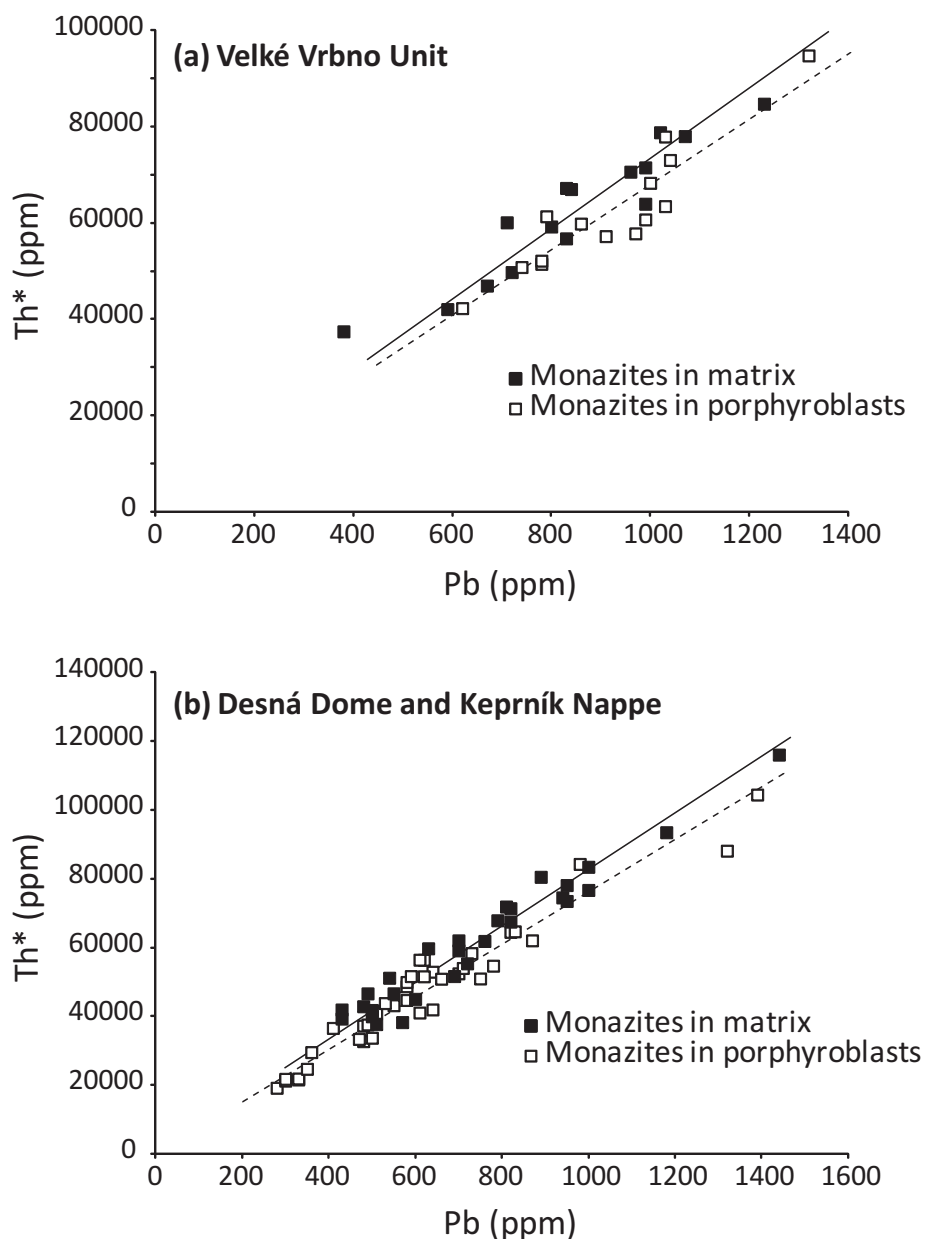


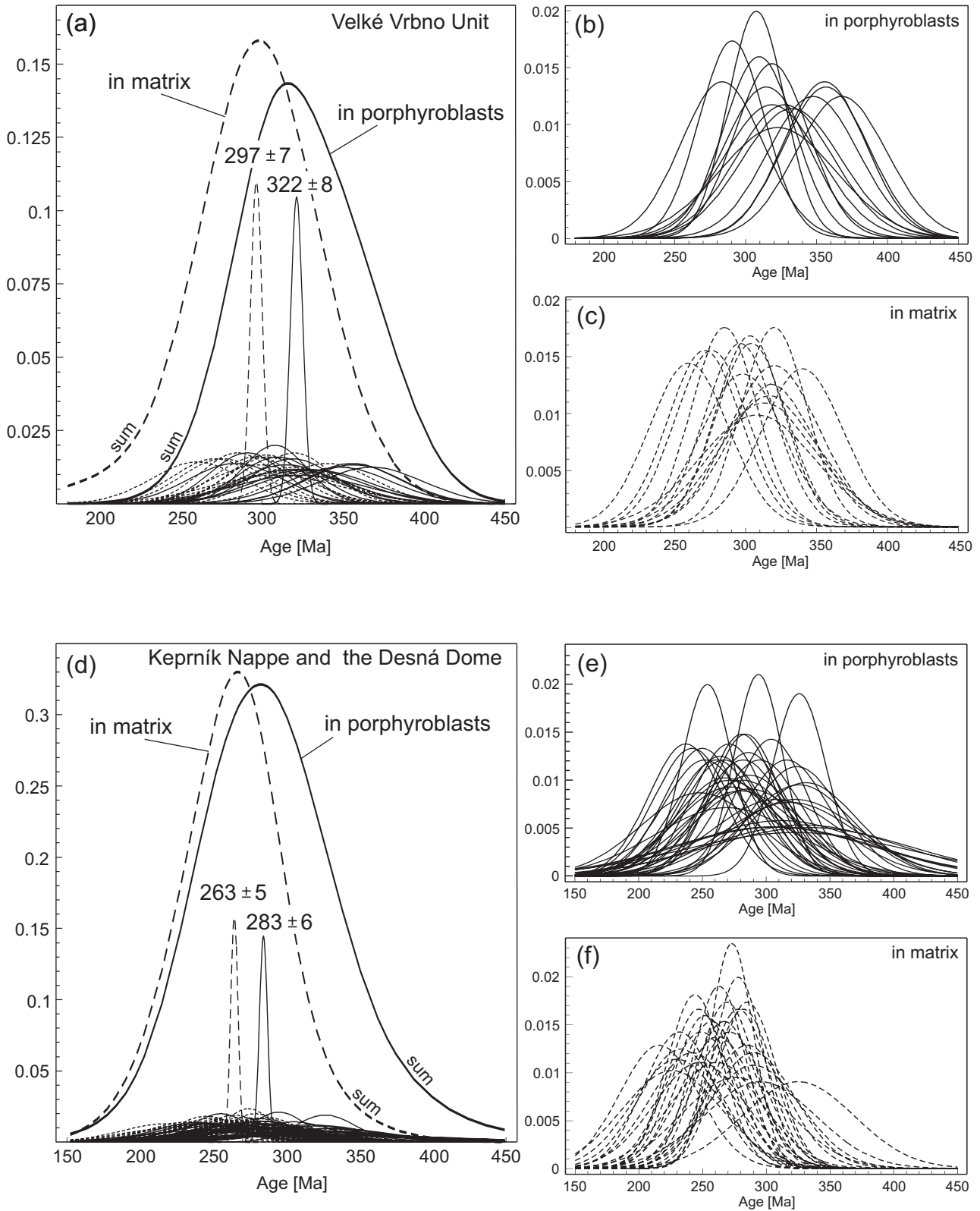
Fig. 7 Isochron diagrams of Pb vs. Th\* contents (ppm) in monazite. Distinguished are monazites located in matrix from those included in garnet–staurolite porphyroblasts, for both the Velké Vrbno Unit (a) and the Keprník Nappe with the Desná Dome (b).

may explain the partial or complete resetting of the U–Th–Pb system in monazite. Therefore, the spread of K–Ar muscovite and biotite and U–Th–Pb monazite ages in the Silesian Domain testifies to the importance of overprinting events subsequent to the last Variscan metamorphic episode and will be discussed below.

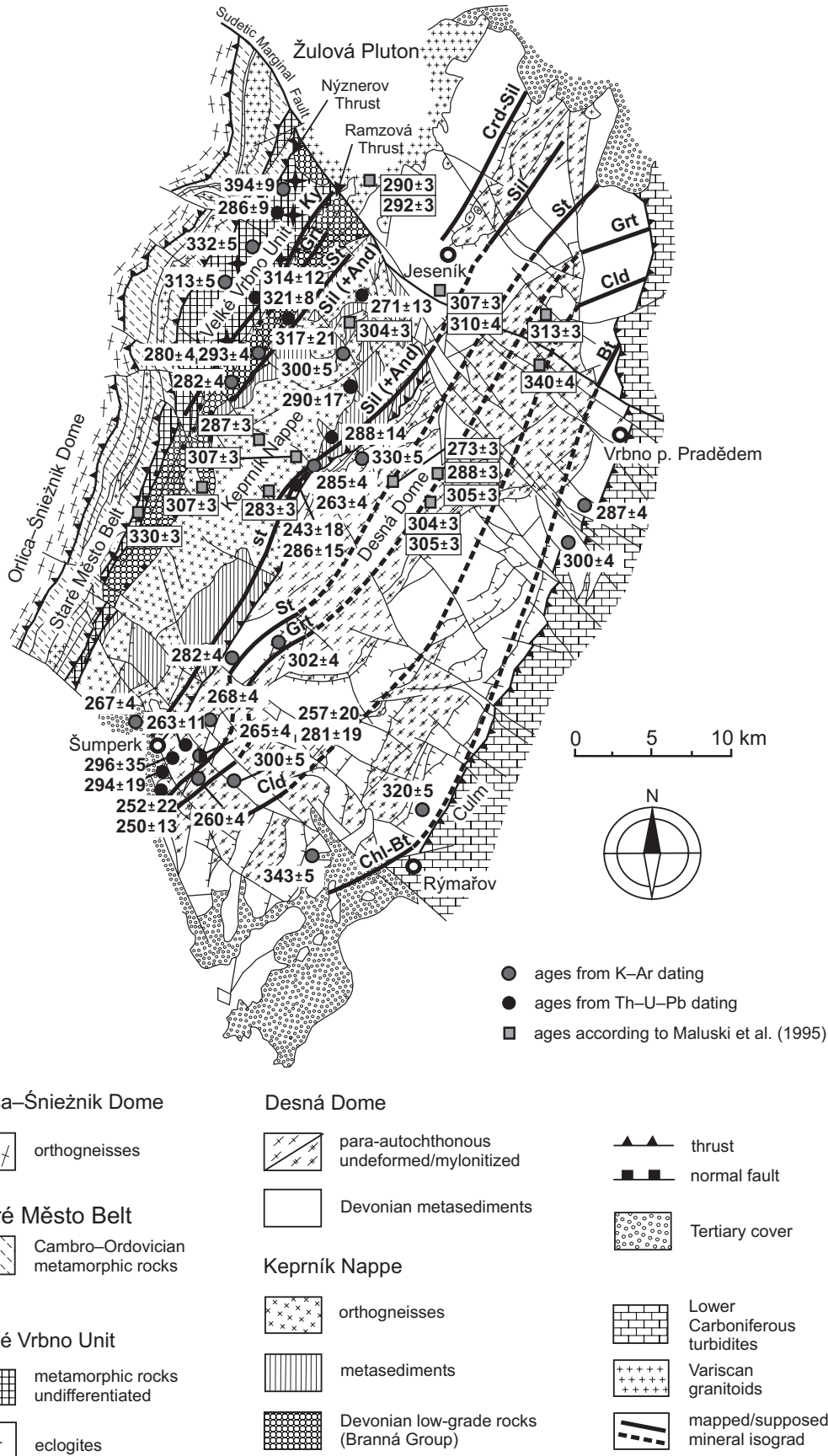
### 5.1.1. Significance of K–Ar ages from the Silesian Domain

Figure 9 shows regional distribution of obtained K–Ar and U–Th–Pb monazite ages as well as existing  $^{40}\text{Ar}$ – $^{39}\text{Ar}$  ages of Maluski et al. (1995). Conventional K–Ar muscovite and biotite ages for samples located in the sillimanite and staurolite zones of the central parts of the

Keprník Nappe and the Desná Dome fall between 290 and 300 Ma, similarly to a range of  $^{40}\text{Ar}$ – $^{39}\text{Ar}$  ages of Maluski et al. (1995). These results are close to cooling ages of  $290 \pm 3$  and  $292 \pm 3$  Ma obtained on biotite and amphibole from the Žulová granite (Maluski et al. 1995). In contrast, the westerly Velké Vrbno Unit reveals cooling ages in between 315 and 332 Ma similarly to the boundary between the Culm basin and the south-eastern margin of the Desná Dome, where K–Ar ages of 340 and 320 Ma were determined (Fig. 9). This regional distribution of K–Ar ages may suggest that the Žulová Pluton played an important role on re-heating and subsequent cooling history of the large part of the Silesian Domain and it is therefore important to estimate the volume and regional extent of this Early Permian intrusion.



**Fig. 8** Probability density functions demonstrating the distribution of the collected single ages from the Velké Vrbno Unit (a–c) and the Keprník Nappe with the Desná Dome (d–f). Each small bell-shaped curve represents a probability density function for one analysis. The thick curves are the sum of all individual curves, representing the accumulated distribution of the measured ages. The narrow peaks show the average ages and corresponding errors in the studied areas. They were obtained statistically assuming the consistency of the samples. In the graphs the data from the matrix and porphyroblasts are shown by solid and dashed curves, respectively.



**Fig. 9** Map of muscovite, biotite and hornblende K–Ar,  $^{40}\text{Ar}$ – $^{39}\text{Ar}$  ages (Maluski et al. 1995) and monazite U–Th–Pb ages from the Silesian Domain. The map shows the regional distribution of Visean (West and East), Westphalian (centre of the Silesian Domain) and Permian ages (SE of the Desná Dome). Abbreviations for names of rock-forming minerals delineating metamorphic isograds according to Kretz (1983).

The gravity surveying places the limit of the Žulová Pluton, characterized by an important gravity low, at the boundary between the Keprník Nappe and the Desná Dome (Zachovalová et al. 2002; Schulmann et al. 2008). In addition there is a number of small granite dykes and apophyses that cross-cut the gneisses of the western part of the Keprník Nappe and which are attributed to the Žulová Pluton. The existence of an important HT event related to the granite intrusion is also supported by LP–HT metamorphism affecting the whole central and western part of the Keprník Nappe and the western part of the Desná Dome (Baratoux et al. 2005; Košuličová and Štípská 2007). We suggest that the geological, geophysical and geochronological dataset is consistent with an important thermal event that affected the significant part of the Silesian Domain due to emplacement of a large granitic mass at *c.* 292 Ma (Laurent et al., this volume). The highest elevation of the pluton is located in the northern part of the studied area, which is also characterized by consistent K–Ar and <sup>40</sup>Ar–<sup>39</sup>Ar cooling ages clustering around 300 Ma, and by the highest intensity of the LP–HT metamorphic overprint.

If we take into consideration the values of biotite and amphibole ages from the Žulová granite, 290 ± 3 and 292 ± 3 Ma, respectively (Maluski et al. 1995), we infer a fast emplacement and cooling, given the large differences in closure temperatures of the two minerals. In the light of this study, it is likely that the Žulová Pluton represents a voluminous magmatic event at around 292 Ma (Laurent et al., this volume) associated with the extensional collapse and development of the large-scale, west-dipping detachment zone. Consequently, the older K–Ar ages from the Velké Vrbno Unit and from the south-eastern part of the Desná Dome may indicate a limited regional extent of this thermal event, and suggest that Early Carboniferous metamorphic ages are preserved only out of the thermal reach of the Žulová granite. The Late Carboniferous to Early Permian magmatism was also reported by Oberc-Dziedzic et al. (2010, 2013) on the example of Strzelin granite further north dated at 300–280 Ma (U–Pb on zircon). These authors show that granite emplacement was controlled by a long-lived ESE–WNW strike-slip fault with a dextral sense of movement. In addition, after the emplacement of the youngest granite, the intrusion underwent brittle deformation associated with broadly N–S directed sinistral displacements.

Permian ages (280–260 Ma) reported from the south-western part of the Desná Dome cannot be correlated with neither the burial–exhumation history nor the thermal event related to the emplacement of the Žulová Pluton (Fig. 9). These ages occur in the domain of important activity of the Sudetic fault system, in particular in the area of ramification of the southern branch of the Sudetic marginal fault (Fig. 2), or potentially of the reach of NNE–SSW trending fault system of the Boskovice Fur-

row (Fig. 1). Therefore, we suggest that the Permian fault systems played an important role in resetting of the K–Ar clocks through facilitating late fluid circulation.

### 5.1.2. Significance of monazite U–Th–Pb ages from the Silesian Domain

The preservation of 322 ± 8 Ma U–Th–Pb ages in monazite included in garnet–staurolite porphyroblasts in the Velké Vrbno Unit (Fig. 8a) indicates that at least this unit contains relics of monazites indicating Visean metamorphism, which corroborates the K–Ar muscovite age of 330 Ma indicative of Visean cooling (Fig. 10). There is a vast majority of U–Th–Pb ages at *c.* 290–300 Ma from the Velké Vrbno Unit matrix monazite and monazite inclusions in garnet and staurolite from the Keprník Nappe and the Desná Dome (Fig. 9). As it is not possible that the S<sub>1</sub> foliation (monazites forming inclusion trails in garnet and staurolite of the Keprník Nappe and the Desná Dome) is younger than the S<sub>2</sub> fabric in adjacent Staré Město Belt (dated at ~340 Ma using syntectonic granitoids by Parry et al. 1997), it is necessary to assume that the age of monazites preserved in the porphyroblasts does not reflect the metamorphic peak leading to the S<sub>1</sub>–S<sub>2</sub> foliations. Monazites included in garnet–staurolite porphyroblasts in metapelites of the Silesian Domain have usually an intermediate Y content (Tab. 2), which means that these monazites predated garnet stabilization. As a consequence, monazites that define the S<sub>1</sub> foliation in porphyroblasts may have crystallized during the prograde Barrovian metamorphism. In the BSE images (Fig. 4c–d) are presented spots with ages varying between ~370 and 335, which is in agreement with recent U–Pb dating of monazite inclusions (350–340 Ma, unpublished data of the authors). Therefore, we suggest that the age of inclusion monazite crystallization is even higher than 322 ± 8 Ma. In contrast, monazites that occur in micaceous layers reveal low-Y contents (Tab. 2), which means that they have crystallized during, or even after, the garnet growth. We suggest that during the intrusion of the voluminous Žulová Pluton and associated D<sub>3</sub> extensional collapse, the fluids penetrated along foliation and intracrystalline fractures, thereby modifying the monazites included in porphyroblasts and matrix. Therefore it seems reasonable to discuss the possible influence of magmatic-related fluids also in the Velké Vrbno Unit which is located closer to the Žulová Pluton than the samples collected in the Keprník Nappe and the Desná Dome. The pervasive flow of late fluids associated with formation of quartz–andalusite-bearing veins is well-documented in the Keprník Nappe and, to a lesser extent, in the Velké Vrbno Unit. The ages of matrix monazites from the Velké Vrbno Unit (314 and 286 Ma) together with some from the Keprník Nappe (290 and

286 Ma) indicate that these units recorded either growth of monazites during the Late Carboniferous plutonic and extensional event or compositional modification of older inherited monazites inherited from the D<sub>2</sub> exhumation event (Fig. 9).

The Permian matrix ages (263 and 252 Ma) recorded by monazites in a south-western part of the Desná Dome and in the eastern part of the Keprník Nappe are located close to faults of regional importance (the possible Permian reactivation of the Keprník Nappe and the Desná Dome interface or the ramification of the Sudetic fault system). In the south-western part of the Desná Dome, it is the boundary Sudetic Fault which strongly affects the basement and its Carboniferous cover. Because monazites bear probable alteration and/or dissolution features (Fig. 3), it is likely that fluids associated with activity of this prominent fault system may have altered the monazite composition during the Permian.

### 5.2. Tectonic implications of various thermal overprints

The Neoproterozoic protolith ages of the Silesian Domain (680–550 Ma, Kröner et al. 2000) (Fig. 10a) show clear affinity to Brunia continent, while Cambro–Ordovician protolith ages (520–490 Ma, Kröner et

al. 2001 for review) of gneisses and volcanites of the OSD and the Staré Město Belt indicate clearly exotic (Saxothuringian) provenance (Mazur et al. 2012; Chopin et al. 2012). Figure 10b shows a regional distribution of U–Th–Pb monazite ages which allow to define two domains with contrasting cooling history: the OSD and the Silesian orogenic wedge. This figure displays a major difference between the monazite ages from the high-grade domain (340–330 Ma) of the OSD and the Silesian Domain including the Velké Vrbno Unit (320–300 Ma) and the Keprník Nappe with the Desná Dome (290–260 Ma). However, the Viséan (321 ± 8 Ma) age of monazites forming S<sub>1</sub> inclusion trails within garnets of the Velké Vrbno Unit, as well as K–Ar ages from the Velké Vrbno Unit and the eastern part of the Desná Dome (332 ± 5 Ma and 340 ± 4, 320 ± 5 Ma, respectively), may indicate that the burial and early exhumation of the Silesian Domain took place during the Early Viséan, similarly to the OSD (Fig. 10). This may suggest that the history of Brunia underthrusting and exhumation of the hot OSD domain were coupled processes as suggested by Schulmann et al. (2008) and Skrzypek et al. (2011). However, relatively high muscovite ages from easterly Devonian slates (Mo 21, Mo 12) may also reflect mixtures of detrital muscovite affected by a metamorphism close to the blocking temperature of the muscovite K–Ar system that was thus

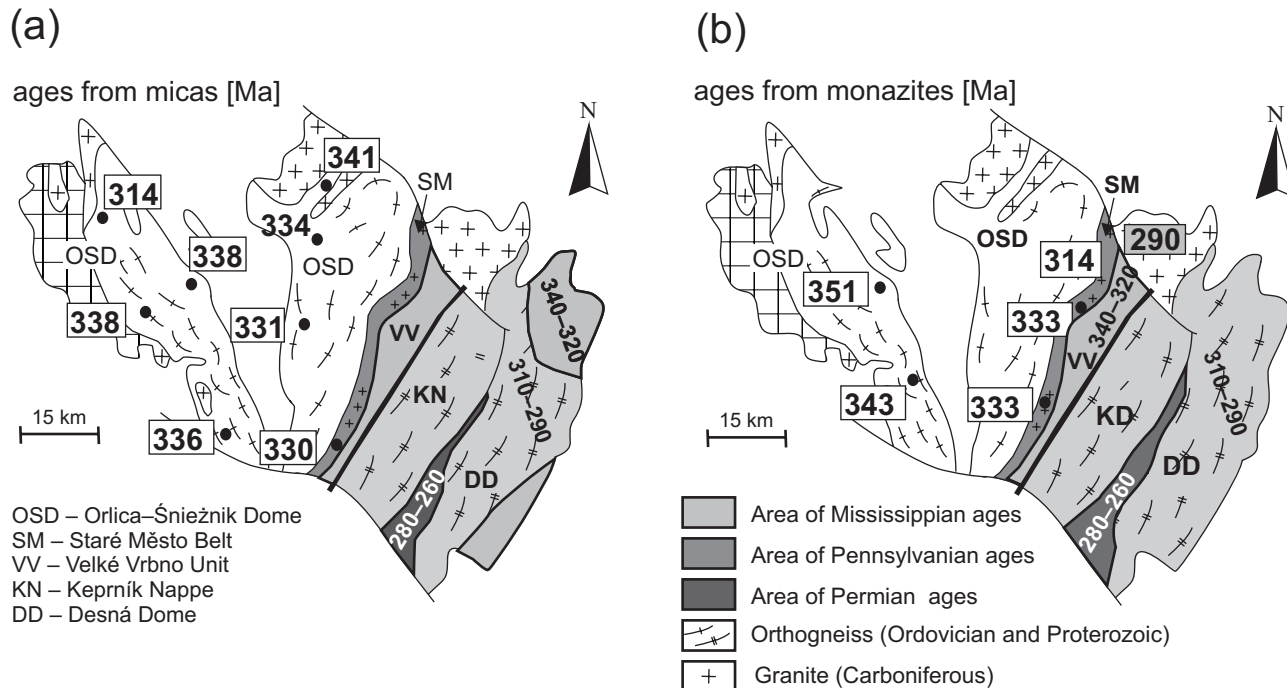


**Fig. 10** Interpretative maps of ages in the Silesian Domain, the Orlica–Śnieżnik Dome and the Staré Město Belt. Shaded area of the external Silesian Domain limited by a thick line to the west represents a domain with comparable data. The limit for individual dating techniques is different (for discussion see text). **a** – Map of representative ages determined using U–Pb method on zircon showing that the two regions are characterized by contrasting protoliths. **b** – Map of representative ages determined from monazites (Silesian Domain: this work; Orlica–Śnieżnik Dome: Gordon et al. 2005; Kusiak et al. 2008).

not entirely reset during the Late Carboniferous thermal event.

The majority of available  $^{40}\text{Ar}$ – $^{39}\text{Ar}$ , K–Ar and U–Th–Pb (CHIME) monazite ages are related to a major Late Carboniferous–Westphalian (~300 Ma) event. This major thermal event was probably related to underplating of the whole Keprník Nappe – and partly also the Desná Dome and the Velké Vrbno Unit – by the large Žulová Pluton dated at ~292 Ma (Laurent et al. this volume). The intrusion was associated with a crustal-scale detachment that operated between the Velké Vrbno Unit and the Keprník Nappe (Fig. 2). The fact that the Westphalian  $^{40}\text{Ar}$ – $^{39}\text{Ar}$  and U–Th–Pb monazite ages are rarely reported from the OSD (Maluski et al. 1995; Gordon et al. 2005) suggests that the Westphalian extension was mainly an intra-Silesian event. However, the Westphalian extension and magmatism were not limited to the Silesian Domain. Late Carboniferous magmatism associated with extensional tectonics occurred west of the OSD (the Karkonosze Pluton) or in the Strzelin Pluton (Oberc-Dziedzic et al. 2013). This extensional tectonics and rapid unroofing of extended crust were expressed by the formation of the Late Carboniferous intra-Sudetic basin and an early activity of the Sudetic transcurrent fault system. This indicates that the lithospheric extension associated with elevated thermal regime affected a significant portion of the Variscan belt in the northern part of the eastern Sudetes, but not the high-grade core of the orogen represented by the OSD. Late Carboniferous magmatic activity was reported from the southern, Bavarian part of the Bohemian Massif, where it was attributed to the activity of the Donau–Pfahl shear zone system (Finger et al. 2007 and references therein) as well as from Erzgebirge–Vogtland magmatic zone in Saxothuringian Domain (Förster and Romer 2010). In conclusion, Late Carboniferous magmatism was a localised process that was associated with NW–SE trending crustal deformation zones cross-cutting the Visean fabric of the Bohemian Massif (Edel et al. 2003, 2013). The only exception represent post-tectonic granites of the Late Carboniferous Erzgebirge–Vogtland magmatic zone that are oriented in NE–SW direction (Förster and Romer 2010).

This study has shown that a number of U–Th–Pb monazite and K–Ar ages are significantly younger in the southern part of the Silesian Domain, mainly close to the Sudetic fault system (Figs 9 and 10b–c). These ages (280–260 Ma) are typically related to the activity of Early to Mid-Permian transcurrent faults affecting the Sudetes (Martínek and Štolfová 2009). In the eastern part of the Variscan belt, the Permian faults are either striking NW–SE or NE–SW and were dated at 288–281 Ma using  $^{40}\text{Ar}$ – $^{39}\text{Ar}$  method (Brandmayr et al. 1995; Büttner 2007), which is consistent with an age of major remagnetization event affecting the whole eastern margin of the Bohemian

Massif (Reisinger et al. 1994). It is namely the Permian Danube NW–SE strike slip system (Brandmayr et al. 1995). In addition, in Permian also formed large basins (Opluštil 2005) associated with extensive volcanism and lamprophyre dyking (Neubauer et al. 2003; Ulrych et al. 2006). Romer et al. (2010) reviewed the post-Variscan deformation and hydrothermal mineralization of the Saxothuringian Domain and showed that the mineralization peak 270–280 Ma includes hydrothermal deposits organized along NE–SW and NW–SE oriented faults. The mineralization and associated formation of numerous grabens in central and western Europe are generally attributed to Early Permian (290–260 Ma) rifting resulting from global post-Variscan plate tectonic reorganization (Ziegler 1993). Therefore, we suppose that the Permian ages in eastern Sudetes, like in Saxothuringian Domain, were related to reactivation of the NW–SE trending dextral Elbe–Sudetic fault system and potential reactivation of NE–SW trending Variscan fabrics during Permian rifting event.

*Acknowledgements.* K. Schulmann acknowledges the Ministry of Education of the Czech Republic (grant LK11202), the French National Grant Agency (ANR DSP-Tibet) and the financial support of CNRS, access to technical facilities of EOST (Strasbourg). Pavla Štípská acknowledges the Czech National Grant Agency (13-16315S). M. Košuličová benefited from financial support of the French embassy during her stays at the University of Strasbourg, France. We thank R. Thuizat (IPGS Strasbourg), N. Clauer (CGS Strasbourg) and A. Wendling (CGS Strasbourg) for help with the K–Ar dating, and J. L. Devidal (LMV Clermont-Ferrand) with the electron-microprobe monazite measurements. Constructive and thorough reviews by two anonymous reviewers as well as excellent editorial work of Friedrich Finger and Vojtěch Janoušek are highly appreciated.

## References

- ANCZKIEWICZ R, SZCZEPAŃSKI J, MAZUR S, STOREY C, CROWLEY Q, VILLA I, THIRLWALL ME, JEFFRIES TE (2007) Lu–Hf geochronology and trace element distribution in garnet: implications for uplift and exhumation of ultra-high pressure granulites in the Sudetes, SW Poland. *Lithos* 95: 363–380
- BAKUN-CZUBAROW N (1998) Ilmenite-bearing eclogites of the West Sudetes – their geochemistry and mineral chemistry. *Arch Mineral* 51: 29–110
- BARATOUX L, LEXA O, COSGROVE J, SCHULMANN K (2005) The quantitative link between fold geometry, mineral fabric and mechanical anisotropy as exemplified by the deformation of amphibolites across a metamorphic gradient. *J Struct Geol* 27: 707–730

- BELL TH, WELCH PW (2002) Prolonged Acadian orogenesis: revelations from foliation intersection axis (FIA) controlled by monazite dating of foliations in porphyroblasts and matrix. *Amer J Sci* 302: 549–581
- BIALEK D, WERNER T (2004) Geochemistry and geochronology of the Javornik granodiorite and its geodynamic significance in the Eastern Variscan Belt. *Geolines* 17: 22–23
- BLACK LP, FITZGERALD JD, HARLEY SL (1984) Pb isotopic composition, colour and microstructure of monazites from a polymetamorphic rock in Antarctica. *Contrib Mineral Petrol* 85: 141–148
- BORKOWSKA M, CHOUKROUNE P, HAMEURT J, MARTINEAU F (1990) A geochemical investigation of the age, significance and structural evolution of the Caledonian–Variscan granite-gneisses of the Śnieżnik metamorphic area (Central Sudetes, Poland). *Geol Sudetica* 15: 1–27
- BOSSE V, BOULVAIS P, GAUTIER P, TIEPOLO M, RUFFET G, DEVIDAL JL, CHERNEVA Z, GERDIKOV I, PAQUETTE JL (2009) Fluid-induced disturbance of the monazite Th–Pb chronometer: in situ dating and element mapping in pegmatites from the Rhodope (Greece, Bulgaria). *Chem Geol* 261: 286–302
- BRANDMAYR M, DALLMEYER RD, HANDLER R, WALLBRECHER E (1995) Conjugate shear zone in the southern Bohemian Massif (Austria): implications for Variscan and Alpine tectonothermal activity. *Tectonophysics* 248: 97–116
- BRÖCKER M, KLEMD R, COSCA M, BROCK W, LARIONOV AN, RODIONOV N (2009) The timing of eclogite facies metamorphism and migmatization in the Orlica–Śnieżnik Complex, Bohemian Massif: constraints from a multimethod geochronological study. *J Metamorph Geol* 27: 385–40
- BRÖCKER M, KLEMD R, KOOLIJMAN E, BERNDT J, LARIONOV A (2010) Zircon geochronology and trace element characteristics of eclogites and granulites from the Orlica–Śnieżnik Complex, Bohemian Massif. *Geol Mag* 147: 339–362
- BÜTTNER SH (2007) Late Variscan stress-field rotation initiating escape tectonics in the south-western Bohemian Massif: a far field response to late orogenic extension. *J Geosci* 52: 29–43
- CATLOS EJ, GILLEY LD, HARRISON TM (2002) Interpretation of monazite ages obtained via in situ analysis. *Chem Geol* 188: 193–215.
- CHÁB J, ŽÁČEK V (1994) Geology of the Žulová Pluton mantle (Bohemian Massif, Central Europe). *Věst Čes geol úst* 69: 1–12
- CHERNIAK DJ, WATSON EB, GROVE M, HARRISON TM (2004) Pb diffusion in monazite: a combined RBS/SIMS study. *Geochim Cosmochim Acta* 68: 829–840
- CHLUPÁČ I (1989) Fossil communities in the metamorphic Lower Devonian of the Hrubý Jeseník Mts., Czechoslovakia. *Neu Jb Geol Paläont, Abh* 177: 367–392
- CHLUPÁČ I (1994) Facies and biogeographic relationships in Devonian of the Bohemian Massif. *Cour Forsch-Inst Senckenberg* 169: 299–317
- CHOPIN F, SCHULMANN K, SKRZYPEK E, LEHMANN J, DUJARDIN JR, MARTELAT JE, LEXA O, CORSINI M, EDEL JB, ŠTÍPSKÁ P, PITRA P (2012) Crustal influx, indentation, ductile thinning and gravity redistribution in a continental wedge: building a Moldanubian mantled gneiss dome with underthrust Saxothuringian material (European Variscan belt). *Tectonics* 31: TC1013
- COPELAND P, PARRISH RR, HARRISON TM (1988) Identification of inherited radiogenic Pb in monazite and its implications for U–Pb systematics. *Nature* 333: 760–763
- COX A, DALRYMPLE GB (1967) Statistical analysis of geomagnetic reversal data and the precision of potassium–argon dating. *J Geophys Res* 72: 2603–2614
- CROWLEY JL, GHENT ED (1999) An electron microprobe study of the U–Th–Pb systematics of metamorphosed monazite: the role of Pb diffusion versus overgrowth and recrystallization. *Chem Geol* 157: 285–302
- DAHL PS (1997) A crystal-chemical basis for Pb retention and fission-track annealing systematics in U-bearing minerals, with implications for geochronology. *Earth Planet Sci Lett* 150: 277–290
- DALLMEYER RD, NEUBAUER F, HÖCK V (1992) Chronology of Late Paleozoic tectonothermal activity in the southeastern Bohemian Massif, Austria (Moldanubian and Moravo–Silesian zones) – Ar<sup>40</sup>/Ar<sup>39</sup> mineral age controls. *Tectonophysics* 210: 135–153
- DODSON MH (1979) Theory of cooling ages. In: JÄGER E, HUNZIKER JC (eds) *Lectures in Isotope Geology*. Springer, New York, pp 194–202
- DON J (1964) The Zlote and Krowiarki mountains as structural elements of the Śnieżnik metamorphic massif. *Geol Sudetica* 1: 79–117
- DON J, SKÁČEL J, GOTOWAŁA R (2003) The boundary zone of the East and West Sudetes on the 1:50 000 scale geological map of the Velké Vrbno, Staré Město and Śnieżnik metamorphic units. *Geol Sudetica* 35: 25–59
- DUDEK A (1980) The crystalline basement block of the Outer Carpathians in Moravia: Bruno Vistulicum. *Rozpr Čs Akad Věd, ř mat příř Věd* 90: 1–85
- EDEL JB, SCHULMANN K, HOLUB FV (2003) Clockwise rotation of the Eastern European Variscides accommodated by dextral lithospheric wrenching: paleomagnetic and structural evidence. *J Geol Soc, London* 160: 209–218
- EDEL JB, SCHULMANN K, SKRZYPEK E, COCHERIE A (2013) Tectonic evolution of the European Variscan belt constrained by palaeomagnetic, structural and anisotropy of magnetic susceptibility data from the Northern Vosges magmatic arc (eastern France). *J Geol Soc, London* 170: 785–804
- FINGER F, GERDES A, JANOUŠEK V, RENÉ M, RIEGLER G (2007) Resolving the Variscan evolution of the Moldanubian sector of the Bohemian Massif: the significance of the Bavarian and the Moravo–Moldanubian tectonometamorphic phases. *J Geosci* 52: 9–28

- FÖRSTER HJ, ROMER RL (2010) Carboniferous magmatism. In: LINNEMANN U, KRONER U, ROMER RL (eds) From the Cadomian Active Margin to the Variscan Orogen: The pre-Mesozoic Geology of Saxo-Thuringia (NW Bohemian Massif). E. Schweizerbart Science Publishers, Stuttgart, pp 287–308
- FRITZ H, DALLMEYER RD, NEUBAUER F (1996) Thick-skinned versus thin-skinned thrusting: rheology-controlled thrust propagation in the Variscan collisional belt (the south-eastern Bohemian Massif, Czech Republic – Austria). *Tectonics* 15: 1389–1413
- GARDÉS E, JAOUŁ O, MONTEL JM, SEYDOUX-GUILLAUME AM, WIRTH R (2006) Pb diffusion in monazite: an experimental study of  $Pb^{2+} + Th^{4+} \leftrightarrow 2Nd^{3+}$  interdiffusion. *Geochim Cosmochim Acta* 70: 2325–2336
- GARDÉS E, MONTEL JM, SEYDOUX-GUILLAUME AM, WIRTH R (2007) Pb diffusion in monazite: new constraints from the experimental study of  $Pb^{2+} \leftrightarrow Ca^{2+}$  interdiffusion. *Geochim Cosmochim Acta* 71: 4036–4043
- GIBSON HD, CARR SD, BROWN RL, HAMILTON MA (2004) Correlations between chemical and age domains in monazite, and metamorphic reactions involving major pelitic phases: an integration of ID-TIMS and SHRIMP geochronology with Y–Th–U X-ray mapping. *Chem Geol* 211: 237–260
- GORDON SM, SCHNEIDER DA, MANECKI M, HOLM DK (2005) Exhumation and metamorphism of an ultrahigh-grade terrane: geochronometric investigations of the Sudete Mountains (Bohemia), Poland and Czech Republic. *J Geol Soc, London* 162: 841–855
- HARTLEY AJ, OTAVA J (2001) Sediment provenance and dispersal in a deep marine foreland basin: the Lower Carboniferous Culm Basin, Czech Republic. *J Geol Soc, London* 158: 137–150
- HEJL E, SEKYRA G, FRIEDL G (2003) Fission-track dating of the south-eastern Bohemian Massif (Waldviertel, Austria): thermochronology and long-term erosion. *Int J Earth Sci* 92: 677–690
- JANOUSEK V, AICHLER J, HANŽL P, GERDES A, ERBAN V, ŽÁČEK V, PECINA V, PUDILOVÁ M, HRDLIČKOVÁ K, MIXA P, ŽÁČKOVÁ E (2014) Constraining genesis and geotectonic setting of metavolcanic complexes: a multidisciplinary study of the Devonian Vrbno Group (Hrubý Jeseník Mts., Czech Republic). *Int J Earth Sci* 103: 455–483
- JASTRZĘBSKI M (2012) New insights into the polyphase evolution of the Variscan suture zone: evidence from the Staré Město Belt, NE Bohemian Massif. *Geol Mag* 149: 945–963
- JASTRZĘBSKI M, ŽELAŽNIEWICZ A, NOWAK I, MURTEZI M, LARIONOV AN (2010) Protolith age and provenance of metasedimentary rocks in Variscan allochthon units: U–Pb SHRIMP zircon data from the Orlica–Śnieżnik Dome, West Sudetes. *Geol Mag* 147: 416–433
- JASTRZĘBSKI M, ŽELAŽNIEWICZ A, MAJKA J, MURTEZI M, BAZARNIK J, KAPITONOV I (2013) Constraints on the Devonian–Carboniferous closure of the Rheic Ocean from a multi-method geochronology study of the Staré Město Belt in the Sudetes (Poland and the Czech Republic). *Lithos* 170–171: 54–72
- KELLY NM, HARLEY SL, MÖLLER A (2012) Complexity in the behavior and recrystallization of monazite during high-T metamorphism and fluid infiltration. *Chem Geol* 322: 192–208
- KLEMD R, BRÖCKER M (1999) Fluid influence on mineral reactions in ultrahigh-pressure granulites: a case study in the Śnieżnik Mts. (West Sudetes, Poland). *Contrib Mineral Petrol* 136: 358–373
- KÖPPEL V, GUNTHER A, GRÜNENFELDER M (1980) Patterns of U–Pb zircon and monazite ages in polymetamorphic units of the Swiss Central Alps. *Schweiz Mineral Petrogr Mitt* 61: 97–119
- KOŠULIČOVÁ M, ŠTÍPSKÁ P (2007) Variations in the transient prograde geothermal gradient from chloritoid–staurolite equilibria: a case study from the Barrovian and Buchan-type domains in the Bohemian Massif. *J Metamorph Geol* 25: 19–36
- KRETZ R (1983) Symbols of rock-forming minerals. *Amer Miner* 68: 277–279
- KRÖNER A, ŠTÍPSKÁ P, SCHULMANN K, JAECKEL P (2000) Chronological constraints on the pre-Variscan evolution of the northeastern margin of the Bohemian Massif, Czech Republic. In: FRANKE W, HAAK V, ONCKEN O, TANNER D (eds) Orogenic Processes: Quantification and Modelling in the Variscan Belt. Geological Society, London, Special Publications 179: 175–197
- KRÖNER A, JÄCKEL P, HEGNER E, OPLETAL M (2001) Single zircon ages and whole rock Nd isotopic systematics of early Palaeozoic granitoid gneisses from the Czech and Polish Sudetes (Jizerské hory, Krkonoše Mountains and Orlice–Śnieżnik Complex). *Int J Earth Sci* 90: 304–324
- KUSIAK MA, SUZUKI K, DUNKLEY DJ, LEKKI J, BAKUN-CZUBAROW N, PASZKOWSKI M, BUDZYŃ B (2008) EPMA and PIXE dating of monazite in granulites from Stary Gieraltów, NE Bohemian Massif, Poland. *Gondwana Res* 14: 675–685
- LANGE U, BRÖCKER M, MEZGER K, DON J (2002) Geochemistry and Rb–Sr geochronology of a ductile shear zone in the Orlica–Śnieżnik Dome (West Sudetes, Poland). *Int J Earth Sci* 91: 1005–1016
- LANGE U, BRÖCKER M, ARMSTRONG R, TRAPP E, MEZGER K (2005) Sm–Nd and U–Pb dating of high-pressure granulites from the Złote and Rychleby Mts (Bohemian Massif, Poland and Czech Republic). *J Metamorph Geol* 23: 133–145
- LAURENT A, JANOUSEK V, MAGNA T, SCHULMANN K, MIKOVÁ J (2014) Petrogenesis and geochronology of a post-collisional calc-alkaline association: the Žulová Pluton, Bohemian Massif. *J Geosci* 59: 415–440
- LEXA O, ŠTÍPSKÁ P, SCHULMANN K, BARATOUX L, KRÖNER A (2005) Contrasting textural record of two distinct meta-

- morphic events of similar P–T conditions and different durations. *J Metamorph Geol* 23: 649–666.
- MALUSKI H, RAJLICH P, SOUČEK J (1995) Pre-Variscan, Variscan and Early Alpine thermo-tectonic history of the north-eastern Bohemian Massif: an  $^{40}\text{Ar}$ – $^{39}\text{Ar}$  study. *Geol Rundsch* 84: 345–358
- MARHEINE D, KACHLÍK V, MALUSKI H, PATOČKA F, ŹELAŹNIEWICZ A (2002) The Ar–Ar age from the West Sudetes (NE Bohemian Massif): constraints on the Variscan polyphase tectonothermal development. In: WINCHESTER JA, PHARAOH TC, VERNIERS J (eds) *Palaeozoic Amalgamation of Central Europe*. Geological Society, London, Special Publications 201: 133–155
- MARTÍNEK K, ŠTOLFOVÁ K (2009) Provenance study of Permian non-marine sandstones and conglomerates of the Krkonoše Piedmont Basin (Czech Republic): exotic marine limestone pebbles, heavy minerals and garnet composition. *Bull Geosci* 84: 555–568
- MAZUR S, SZCZEPAŃSKI J, TURNIAK K, MCNAUGHTON NJ (2012) Location of the Rheic suture in the eastern Bohemian Massif: evidence from detrital zircon data. *Terra Nova* 24: 199–206
- MCDUGALL I, HARRISON IM (1988) *Geochronology and Thermochronology by the  $^{40}\text{Ar}/^{39}\text{Ar}$  Method*. Oxford University Press, Oxford, pp 1–212
- MONTEL JM, FORET S, VESCHAMBRE M, NICOLLET C, PROVOST A (1996) Electron microprobe dating of monazite. *Chem Geol* 131: 37–53
- NEUBAUER F, DALLMEYER RD, FRITZ H (2003) Chronological constraints of late- and post-orogenic emplacement of lamprophyre dykes in the southeastern Bohemian Massif, Austria. *Schweiz Mineral Petrograph Mitt* 83: 317–330
- OBERC-DZIEDZIC T, KRYZA R, BIALEK J (2010) Variscan multistage granitoid magmatism in Brunovistulicum: petrological and SHRIMP U–Pb zircon geochronological evidence from the southern part of the Strzelin Massif, SW Poland. *Geol Q* 54: 301–324
- OBERC-DZIEDZIC T, KRYZA R, PIN C, MADEJ S (2013) Sequential granite emplacement: a structural study of the late Variscan Strzelin intrusion, SW Poland. *Int J Earth Sci* 102: 1289–1304
- OPLUŠTIL S (2005) The effect of paleotopography, tectonics and sediment supply on quality of coal seams in continental basins of central and western Bohemia (Westphalian). Czech Republic. *Int J Coal Geol* 64: 173–203
- PARRISH R (1990) U–Pb dating of monazite and its applications to geological problems. *Can J Earth Sci* 17: 1431–1450
- PARRY M, ŠTÍPSKÁ P, SCHULMANN K, HROUDA F, JEŽEK J, KRÖNER A (1997) Tonalite sill emplacement at an oblique plate boundary: northeastern margin of the Bohemian Massif. *Tectonophysics* 280: 61–81
- PATOČKA F (1987) The geochemistry of mafic metavolcanics: implications for the origin of the Devonian massive sulfide deposits at Zlaté Hory, Czechoslovakia. *Miner Depos* 22: 144–150
- POITRASSON F, CHENERY S, BLAND DJ (1996) Contrasted monazite hydrothermal alteration mechanisms and their geochemical implications. *Earth Planet Sci Lett* 145: 79–96
- POITRASSON F, CHENERY S, SHEPHERD TJ (2000) Electron microprobe and LA-ICP-MS study of monazite hydrothermal alteration: implications for U–Th–Pb geochronology and nuclear ceramics. *Geochim Cosmochim Acta* 64: 3283–3297
- REISINGER J, EDEL JB, MAURITSCH HJ (1994) Late Carboniferous–Late Permian paleomagnetic overprinting of Carboniferous granitoids in southern Bohemian Massif (Austria). *Phys Earth Planet Inter* 85: 53–65
- ROMER RL, SCHNEIDER J, LINNEMANN U (2010) Post-Variscan deformation and hydrothermal mineralization in Saxo-Thuringia and beyond: a geochronological review. In: LINNEMANN U, KRONER U, ROMER RL (eds) *From the Cadomian Active Margin to the Variscan Orogen: The pre-Mesozoic Geology of Saxo-Thuringia (NW Bohemian Massif)*. E. Schweizerbart Science Publishers, Stuttgart, pp 347–360
- SCHNEIDER DA, ZAHNISER SJ, GLASOCK JM, GORDON SM, MANECKI M (2006) Thermochronology of the west Sudetes (Bohemian Massif): rapid and repeated exhumation in the eastern Variscides, Poland and Czech Republic. *Amer J Sci* 306: 846–873
- SCHULMANN K, GAYER R (2000) A model for a continental accretionary wedge developed by oblique collision: the NE Bohemian Massif. *J Geol Soc, London* 157: 401–416
- SCHULMANN K, MELKA R, LOBKOWICZ M, LEDRU P, LARDEAUX JM, AUTRAN A (1994) Contrasting styles of deformation during progressive nappe stacking at the southeastern margin of the Bohemian Massif (Thaya Dome). *J Struct Geol* 16: 355–370
- SCHULMANN K, LEXA O, ŠTÍPSKÁ P, RACEK M, TAJČMANOVÁ L, KONOPÁSEK J, EDEL J.-B, PESCHLER A, LEHMANN J (2008) Vertical extrusion and horizontal channel flow of orogenic lower crust: key exhumation mechanisms in large hot orogens? *J Metamorph Geol* 26: 273–297
- SKRZYPEK E, ŠTÍPSKÁ P, SCHULMANN K, LEXA O, LEXO VÁ M (2011) Prograde and retrograde metamorphic fabrics – a key for understanding burial and exhumation in orogens (Bohemian Massif). *J Metamorph Geol* 29: 451–472
- SEYDOUX-GUILLAUME AM, PAQUETTE JL, WIEDENBECK M, MONTEL JM, HEINRICH W (2002) Experimental resetting of the U–Th–Pb systems in monazite. *Chem Geol* 191: 165–181
- SOUČEK J (1978) Metamorphic zones of the Vrnbno and Rejvíz series, the Hrubý Jeseník Mountains, Czechoslovakia. *Tschermaks mineral petrogr Mitt* 25: 195–217
- SOUČEK J (1981) Geochemistry of the Devonian metabasites from the high and low Jeseník Mountains. *Čas Mineral Geol* 265: 125–142

- STEIGER R, JAEGER E (1977) Subcommittee on Geochronology: convention on the use of decay constants in geo- and cosmochronology. *Earth Planet Sci Lett* 36: 359–362
- STELTENPOHL MG, CYMERMAN Z, KROGH EJ, KUNK MJ (1993) Exhumation of eclogitized continental basement during Variscan lithospheric delamination and gravitational collapse, Sudetes Mountains, Poland. *Geology* 21: 1111–1114
- ŠTÍPSKÁ P, SCHULMANN K (1995) Inverted metamorphic zonation in a basement-derived nappe sequence, eastern margin of the Bohemian Massif. *Geol J* 30: 385–413
- ŠTÍPSKÁ P, SCHULMANN K, HÖCK V (2000) Complex metamorphic zonation of the Thaya Dome: result of buckling and gravitational collapse of imbricated nappe sequence. In: COSGROWE JW, AMEEN MS (eds) *Forced Folds and Fractures*. Geological Society, London, Special Publications 169: 197–211
- ŠTÍPSKÁ P, SCHULMANN K, THOMPSON AB, JEŽEK J, KRÖNER A (2001) Thermomechanical role of a Cambro–Ordovician paleorift during the Variscan collision: the NE margin of the Bohemian Massif. *Tectonophysics* 332: 239–253
- ŠTÍPSKÁ P, SCHULMANN K, KRÖNER A (2004) Vertical extrusion and middle crustal spreading of omphacite granulite: a model of syn-convergent exhumation (Bohemian Massif, Czech Republic). *J Metamorph Geol* 22: 179–198
- ŠTÍPSKÁ P, PITRA P, POWELL R (2006) Separate or shared metamorphic histories of eclogites and surrounding rocks? An example from the Bohemian Massif. *J Metamorph Geol* 24: 219–240
- ŠTÍPSKÁ P, CHOPIN F, SKRZYPEK E, SCHULMANN K, LEXA O, PITRA P, MARTELAT JE, BOLINGER C, ŽÁČKOVÁ E (2012) The juxtaposition of eclogite and mid-crustal rocks in the Orlica–Šniežnik Dome, Bohemian Massif. *J Metamorph Geol* 30: 213–234
- SUESS FE (1912) Die moravische Fenster und ihre Beziehung zum Grundgebirge des Hohen Gesenkes. *Denkschr Österr Akad Wiss Mat Naturwiss Kl* 88: 541–631
- SUESS FE (1926) *Intrusionstektonik und Wandertektonik im variszischen Grundgebirge*. Bornträger, Berlin, pp 1–269
- SUZUKI K, ADACHI M (1991) The chemical Th–U–total Pb isochron ages of zircon and monazite from the Gray Granite of the Hida Terrane, Japan. *J Earth Sci Nagoya Univ* 38: 11–38
- SUZUKI K, ADACHI M, KAJIZUKA I (1994) Electron microprobe observations of Pb diffusion in metamorphosed detrital monazites. *Earth Planet Sci Lett* 128: 391–405
- ULRICH S, SCHULMANN K, CASEY M (2002) Microstructural evolution and rheological behaviour of marbles deformed at different crustal levels. *J Struct Geol* 24: 979–995
- ULRYCH J, PEŠEK J, ŠTEPÁNKOVÁ-SVOBODOVÁ J, BOSÁK P, LLOYD FE, VON SECKENDORFF V, LANG M, NOVÁK JK (2006) Permo–Carboniferous volcanism in late Variscan continental basins of the Bohemian Massif (Czech Republic): geochemical characteristic. *Chemie der Erde – Geochemistry* 66: 37–56
- TURNIAK K, MAZUR S, WYSOCZANSKI R (2000) SHRIMP zircon geochronology and geochemistry of the Orlica–Šniežnik gneisses (Variscan belt of Central Europe) and their tectonic implications. *Geodin Acta* 13: 1–20
- VAN BREEMEN O, AFTALION M, BOWES DR, DUDEK A, MISAŘ Z, POVONDRA P, VRÁNA S (1982) Geochronological studies of the Bohemian Massif, Czechoslovakia, and their significance in the evolution Central Europe. *Trans Roy Soc Edinb, Earth Sci* 73: 89–108
- VILLA IM (1997) Isotopic closure. *Terra Nova* 10: 42–47
- WILLIAMS ML, JERCINOVIC MJ, HARLOV DE, BUDZYŃ B, HETHERINGTON C (2011) Resetting monazite ages during fluid-related alteration. *Chem Geol* 283: 218–225
- ZACHOVALOVÁ K, LEICHMANN J, ŠVANCARA J (2002) Žulová Batholith: a post-orogenic, fractionated ilmenite–allanite I-type granite. *J Czech Geol Soc* 47: 35–44
- ZIEGLER PA (1993) Late-Paleozoic–Early Mesozoic plate reorganization: evolution and demise of the Variscan fold belt. In: VON RAUMER JF, NEUBAUER F (eds) *Pre-Mesozoic Geology of the Alps*. Springer, Berlin, pp 203–216
- ŽÁČEK V (1996) Retrograded eclogite from the Staré Město Belt, NE margin of the Bohemian Massif. *J Czech Geol Soc* 41: 167–175